Lithos 140–141 (2012) 103–118

Contents lists available at SciVerse ScienceDirect

Lithos

journal homepage: www.elsevier.com/locate/lithos

Northwestern Junggar Basin, Xiemisitai Mountains, China: A geochemical and geochronological approach

Ping Shen [a,*], Yuanchao Shen [a], Xian-Hua Li [a], Hongdi Pan [b], Heping Zhu [a], Lei Meng [a], Huawu Dai [a]

[a] Key Laboratory of Mineral Resources, Institute of Geology and Geophysics, Chinese Academy of Sciences, Beijing 100029, China
[b] Collage of Earth Sciences, Chang'an University, Xi'an 710054, China

ARTICLE INFO

Article history:
Received 6 July 2011
Accepted 3 February 2012
Available online 14 February 2012

Keywords:
Volcanic rocks
Sr–Nd–Pb isotopes
SIMS zircon U–Pb dating
Xiemisitai Mountains
West Junggar Region
Xinjiang

ABSTRACT

We report SIMS U–Pb zircon, elemental and Nd–Sr–Pb isotopic data for the volcanic rocks and their subvolcanic units from the Xiemisitai Mountains in the West Junggar Region (Xinjiang, China), aiming to determine their ages, source regions and tectonic setting. Zircon U–Pb dating results of the volcanic rocks (422.5 ± 1.9 Ma–411.2 ± 2.9 Ma) indicate that the volcanic strata occurred in the Xiemisitai Mountains at Late Silurian–Early Devonian time rather than Middle Devonian as suggested previously. They are probably the eastern extension of the early Paleozoic (Cambrian–Silurian) Boshchekul–Chingiz volcanic arc of East Kazakhstan in China.

The Xiemisitai volcanic rocks include andesite, rhyolite, and their pyroclastic equivalents. The subvolcanic units are felsite and granite porphyry. Andesite is moderately LREE-enriched, with a marked negative Nb anomaly and Th/Yb-enrichment. Rhyolite, felsite and granite porphyry are enriched in LREE and Th and depleted Nb. The initial Sr isotope values of the Xiemisitai volcanic rocks and their subvolcanic units range from 0.702294 to 0.704456, ε_{Nd}(420 Ma) from +0.19 to +1.88 with Nd model ages ranging from 600 to 803 Ma. Initial Pb isotope ratios ($^{206}Pb/^{204}Pb$) are 17.77–17.96, ($^{207}Pb/^{204}Pb$) are 15.49–15.54 and ($^{208}Pb/^{204}Pb$) are 37.56–37.80. These features suggest that the Xiemisitai volcanic rocks and their subvolcanic units derived from a mantle wedge significant mixed by subducted material (EMI) in a subduction zone. They also indicate significant involvement of Neoproterozoic primitive crust in the formation of the Xiemisitai magmatic arc. These rocks are associated with a Late Silurian–Early Devonian southward subduction of the oceanic lithosphere in the northern West Junggar Region. This gives rise to an EW-trending Boshchekul–Chingiz volcanic arc and associated metallogenic belt in the northern West Junggar Region and adjacent Kazakhstan.

1. Introduction

The Central Asian Orogenic Belt (CAOB) is bordered on the north by the Siberian craton and on the south by the North China–Tarim craton, extending from the Urals in the west, through Uzbekistan, Tajikistan, Kyrgyzstan, and Kazakhstan, northwest China, Mongolia, and northeast China to the Russian Far East (Fig. 1a, Sengör et al., 1993; Windley et al., 2007; Xiao et al., 2008, 2009). The CAOB is a giant accretionary orogen with the highest rate of Phanerozoic continental growth (Windley et al., 2007; Xiao et al., 2009, 2010) and significant metallogenic importance (He et al., 2004; Heinhorst et al., 2000; Kudryavtsev, 1996).

The West Junggar Region in Xinjiang (China) is an important part of the CAOB and is bounded by the Altai orogen (southern margin of the Siberian Craton) to the north and by the Tianshan orogen (northern margin of Tarim Craton) to the south (Fig. 1b). It is the Chinese prolongation of the Kazakhstan orogenic belt (e.g., He et al., 2004; Windley et al., 2007; Xiao et al., 2009), and is largely composed by Paleozoic volcanic arcs in the north and accretionary complexes in the south (e.g., Windley et al., 2007; Xiao et al., 2008; Zhang et al., 2011). They were accreted onto the Kazakhstan plate as the Tarim, Kazakhstan and Siberian plates converged (Chen and Arakawa, 2005; Xiao et al., 2008). This geodynamic process led to the formation of volcanic- and intrusion-related gold deposits (Shen and Jin, 1993; Shen et al., 2007, 2008a,b) and porphyry copper deposits in the West Junggar Region (Shen et al., 2009, 2010a,b; Zhang et al., 2006).

The northern West Junggar Region and adjacent East Kazakhstan mainly involves the northwest–southeast trending Zharma–Saur and Boshchekul–Chingiz volcanic arcs from north to south with their Paleozoic lithostratigraphy ranging from Cambrian to Permian in age (Fig. 1b). It is undoubted that a suite of Devonian and Carboniferous volcano-sedimentary strata continuously extend from the Saur Mountains in the West Junggar Region of China to the Zharma–Saur Mountains in Kazakhstan (Fig. 1b). It is also possible

* Corresponding author. Tel.: +86 10 82998189; fax: +86 10 62010846.
E-mail address: pshen@mail.iggcas.ac.cn (P. Shen).

0024-4937/$ – see front matter.
doi:10.1016/j.lithos.2012.02.004

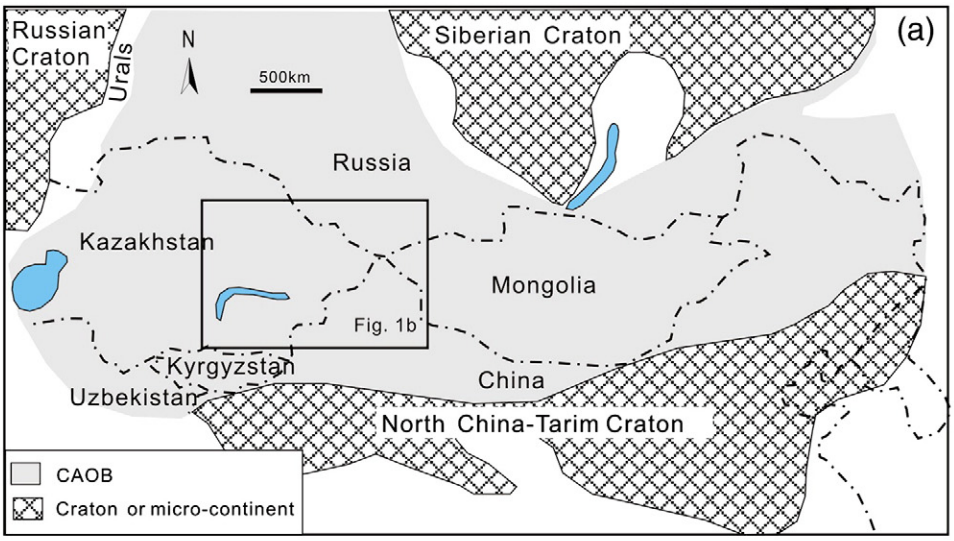
(a)
Russian Craton
Urals
N
500km
Siberian Craton
Russia
Kazakhstan
Mongolia
Fig. 1b
Kyrgyzstan
Uzbekistan
China
North China-Tarim Craton
CAOB
Craton or micro-continent

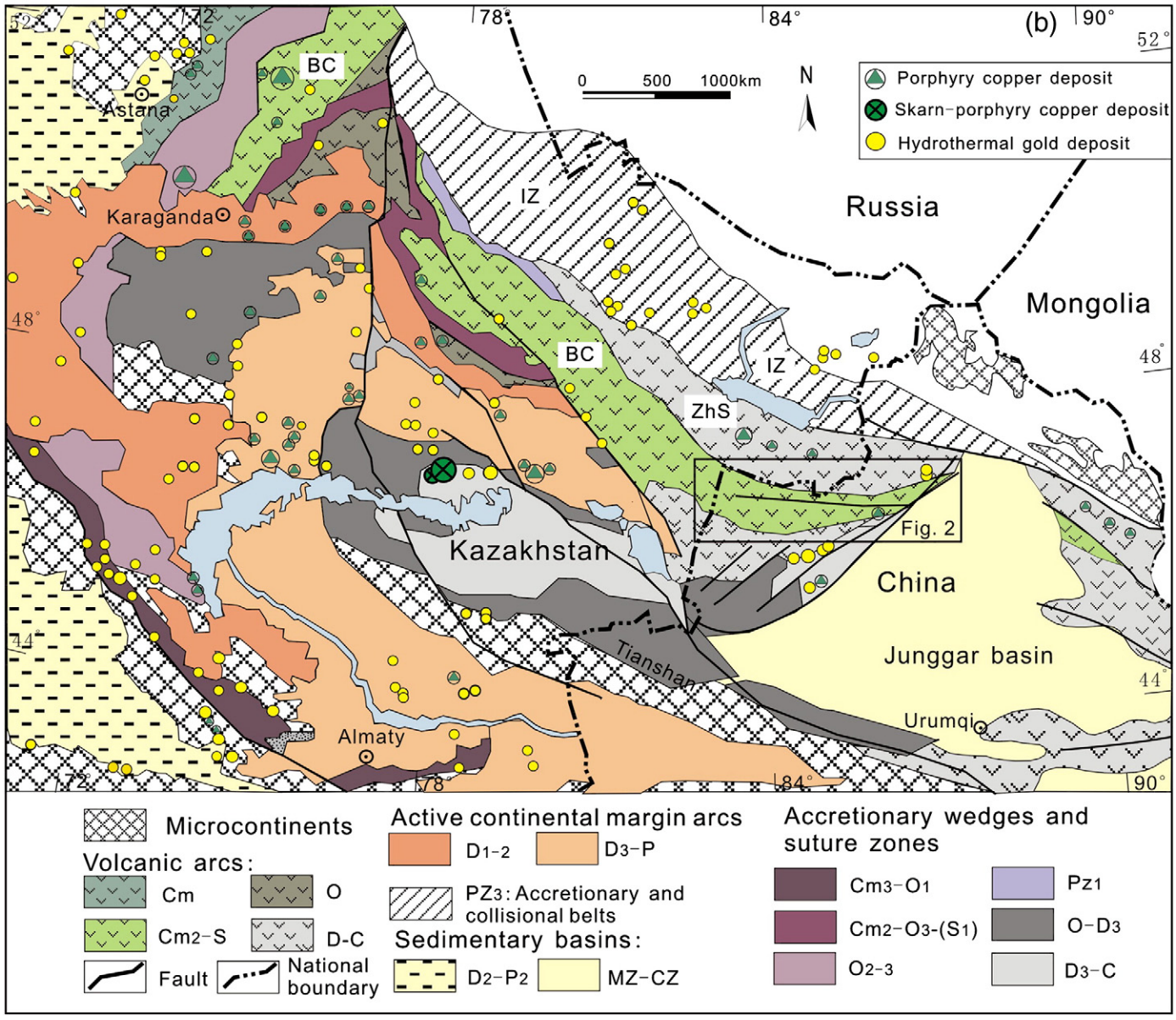
(b)
72°
78°
84°
90°
52°
48°
44°
0 500 1000km
N
Porphyry copper deposit
Skarn-porphyry copper deposit
Hydrothermal gold deposit
BC
Astana
Karaganda
IZ
Russia
Mongolia
ZhS
Fig. 2
Kazakhstan
China
Junggar basin
Tianshan
Urumqi
Almaty
Microcontinents
Volcanic arcs:
Cm
O
Cm2–S
D-C
Fault
National boundary
Active continental margin arcs
D1-2
D3–P
PZ3: Accretionary and collisional belts
Sedimentary basins:
D2–P2
MZ–CZ
Accretionary wedges and suture zones
Cm3–O1
Pz1
Cm2–O3-(S1)
O–D3
O2-3
D3–C

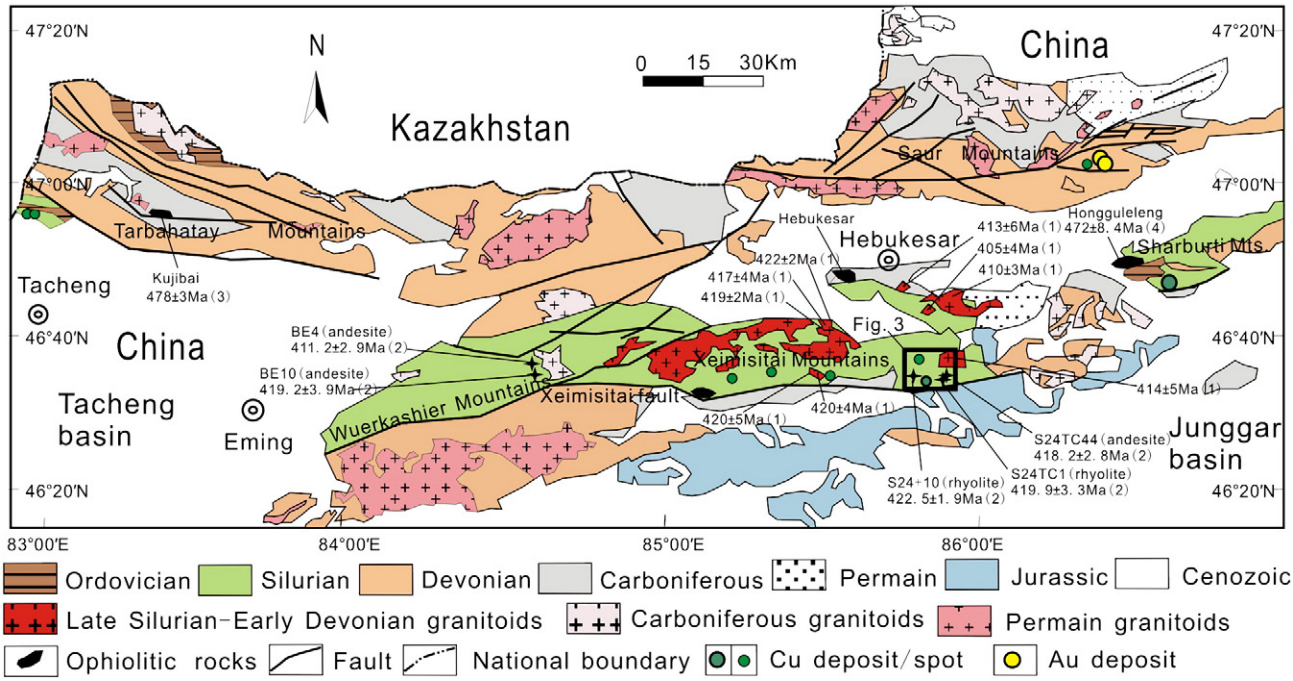

Fig. 2. Generalized geological map of the northern West Junggar Region (modified after BGMRXUAR, 1993; Chen et al., 2010). Age data are from 1 — Chen et al. (2010), 2 — This study, 3 — Zhu and Xu (2006), and 4 — Zhang and Guo (2010).

that the Boshchekul–Chingiz volcanic arc extends eastward to the West Junggar Region of China, but where this early Paleozoic (Cambrian to Silurian) volcanic arc continues in West Junggar Region is controversial (He et al., 2004; Wang, 1996; Windley et al., 2007; Xiao et al., 2008) and needs further detailed studies. Plutons with SHRIMP and LAICP-MS zircon U–Pb ages ranging from 422 to 405 Ma were reported from the Xiemisitai Mountains in the northern West Junggar Region (Chen et al., 2010). The relationship between the plutons and the volcanic rocks implies that the volcanic rocks occurred in the Xiemisitai Mountains may not be fossil-dated Middle Devonian as suggested previously (BGMRXUAR, 1993). Moreover, previous researchers suggested that the volcanic rocks in the Xiemisitai Mountains occurred in Devonian–Carboniferous island arc setting (He et al., 2004; Wang, 1996) supported by minor geochemical data. Therefore, much more geochemical work is needed to clarify the source regions and tectonic setting for the volcanic rocks in the Xiemisitai Mountains. Most important, in East Kazakhstan, many ore deposits (e.g. Pyritic–Cu–Zn polymetallic deposit, porphyry copper deposits and lode gold deposits), widespread in the Boshchekul–Chingiz volcanic arc, are forming the Boshchekul–Chingiz metallogenic belt (Fig. 1b) and may represent manifestations of specific geodynamic environments (Seltmann and Porter, 2005; Shatov et al., 1996). In China, many copper occurrences are recognized in the southern slope of the Tarbgatay, Xiemisitai and Sharburti Mountains (Fig. 2). Recently, local geological team explored and discovered the Hongguleleng volcanic-related copper deposit in the Sharburti Mountains and we mapped and discovered the volcanic- and subvolcanic rocks-related copper deposit and occurrences in the Xiemisitai Mountains (Fig. 2, Shen et al., 2010c). The copper mineralization in the north West Junggar Region is controlled by a caldera fracture systems superimposed by the regional faults. Therefore, it is possible that the northern West Junggar Region may contain significant metallogenic occurrences importance and may be correlated with the Boshchekul–Chingiz metallogenic belt in East Kazakhstan. It is necessary to study the chronology, source regions and tectonic setting of the volcanic rocks and their subvolcanic units recognized in the Xiemisitai Mountains in order to identify the extend of the early Paleozoic (Cambrian to Silurian) Boshchekul–Chingiz volcanic arc and associated metallogenic belt in China.

Previous discussions about the chronology, tectonic setting, source regions and associated mineralization of the West Junggar Region were mainly focused on the southern West Junggar Region (Han et al., 2006; Shen and Jin, 1993; Shen et al., 2009, 2010a,b; Xiao et al., 2008; Zhang et al., 2011). In this paper, we have mapped volcanic rocks and their subvolcanic units over 20 km^2 of the Xiemisitai Mountains and first report the results of 42 whole-rock major and trace element analyses, 10 Nd isotope ratios, 6 Sr and Pb isotope ratios and five SIMS zircon U–Pb dating on volcanic rocks and their subvolcanic units occurring in the Xiemisitai Mountains, the northern West Junggar Region, China. Those new data have significant implications for the understanding of the Paleozoic continental growth of CAOB and the associated mineralization of West Junggar Region, China and adjacent East Kazakhstan.

2. Geological outline

The northern West Junggar Region is located between latitudes 46°20′ and 47°20′ north and longitudes 83°00′ and 87°00′ east and includes several east–west striking mountains: Tarbgatay, Saur, Xiemisitai, Sharburti and Wuerkashier Mountains (Fig. 2). Geologically, the northern West Junggar Region is characterized by EW-trending faults and fault-bounded blocks. This is very different from the southern West Junggar Region, where major faults and fault-bounded accretionary complexes are mainly NE–SW oriented (Fig. 1b).

Fig. 1. (a) North Xinjiang in the Central Asia Orogenic Belt (after Xiao et al., 2009); (b) Simplified geotectonic map of the Paleozoic of Kazakhstan and contiguous China (modified after He et al., 2004; Windley et al., 2007; Xiao et al., 2008; Abdulin and Esenov, 1975; Abdulin et al., 1996 and other sources). Cm, Cambrian; O, Ordovician; S, Silurian; D, Devonian; C, Carboniferous; P, Permian; PZ, Paleozoic; MZ, Mesozoic; CZ, Cenozoic. Subscripts 1, 2, 3 refer to Early, Middle, Late. BC, Boshchekul–Chingiz volcanic arcs; ZhS, Zharma–Saur volcanic arcs; IZ, Irtysh–Zaisan accretionary and collisional belts.

Table 1
Paleozoic lithostratigraphy of the northern West Junggar Region.

Period	Group	Rock types	Basis for period
Permian	Kalagang Group	Basalt, rhyolite, andesite, tuff and tuffaceous sandstone	280 ± 2–283 ± 2 Ma (whole rock Ar–Ar) (Zhou et al., 2008)
	Harjiawu Group	Andesite, basalt, tuff and tuffaceous sandstone	296.7 Ma (whole rock Ar–Ar) (Zhou et al., 2008)
Carboniferous	Hebukehe Group	Conglomerate, sandstone, siltstone and felsic volcanic pyroclastic rocks	Fossil and stratigraphic correlation
	Heishantou Group	Basic-intermediate volcanic rocks, and pyroclastic rocks	343 ± 22 Ma (whole rock Rb–Sr) (Liu et al., 2003)
Devonian	Tarbahatay Group	Volcanic rocks, sandstone, and tuff	Fossil and stratigraphic correlation
	Saurshan Group	Tuffaceous sandstone, mudstone with andesite and limestone interlayers	Fossil and stratigraphic correlation
	Kulumudi Group	Sandy conglomerate, siltstone, limestone, and volcanic rocks	Fossil and stratigraphic correlation
	Hujiersite Group	Volcanic breccia, andesite porphyry, rhyolite, and andesitic tuff	Fossil and stratigraphic correlation
	Mangkelu Group	Siltstone, limestone, and mudstone	Fossil and stratigraphic correlation
Silurian	Kekexionghuduke Group	Tuffaceous siltstone and tuffaceous sandstone	Fossil and stratigraphic correlation
	Sharbur Group	Tuffaceous sandstone, sandstone, limestone, and volcanic rocks	Fossil and stratigraphic correlation
Ordovician	Kekeshayi Group	Basalt, andesite, tuff and siliceous rocks	Fossil and stratigraphic correlation

The Paleozoic lithostratigraphy of the northern West Junggar Region ranges in age from Ordovician to Permian (Fig. 2) and is summarized in Table 1. The fossil-dated Ordovician and Silurian strata only occur in the Sharburti Mountains and in the Tarbgatay Mountains close to the border of China–Kazakhstan (Fig. 2; BGMRXUAR, 1993). The fossil- and isotope-dated Devonian and Carboniferous strata widely occur in the northern West Junggar Region (Fig. 2; BGMRXUAR, 1993). The whole rock Rb–Sr age of the Heishantou Group andesite occurred in the Saur Mountains is 343 ± 22 Ma (Liu et al., 2003). The isotope-dated Permian strata scattered in the northern West Junggar Region (Fig. 2; BGMRXUAR, 1993). The whole rock Ar–Ar ages of the Kalagang Group volcanic rocks occurred in the Saur Mountains range from 280 ± 2 to 283 ± 2 Ma (Zhou et al., 2008).

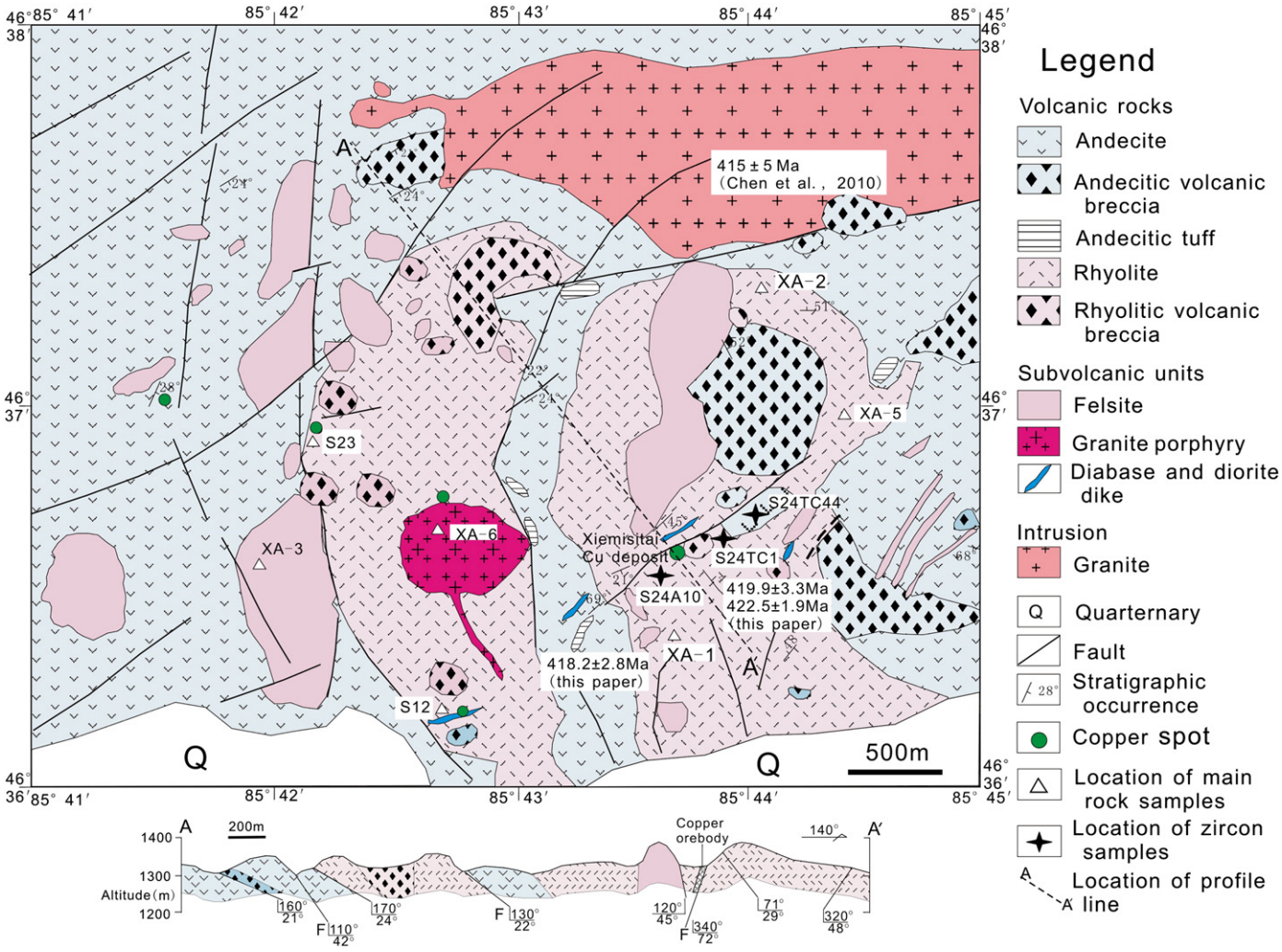

Fig. 3. Geological map of the Late Silurian volcanic rocks and their subvolcanic units (in relative age sequence, oldest at top in legend) from the east part of the Xiemisitai Mountains in the northern West Junggar (mapped by authors). It also shows profile through the studied area and locations of main samples and the Xiemisitai copper deposit.

The northern West Junggar Region is characterized by the occurrence of Hongguleleng ophiolite belt (Fig. 2). The belt includes the Hongguleleng, Hebukesaier, Kujibai ophiolites from east to west (Fig. 2, IGCAGS, 2006; Zhu and Xu, 2006). The Hongguleleng ophiolite, the easternmost fragment of the ophiolite belt (Fig. 2), is composed of serpentinized peridotite and gabbro, whose gabbro yielded a SHRIMP zircon U–Pb age of 472 ± 8.4 Ma (Zhang and Guo, 2010). Newly-discovered Kujibai ophiolite, the westernmost fragment of the ophiolite belt (Fig. 2), consists of gabbro, serpentinized peridotite and siliceous rocks. The gabbro yielded a SHRIMP zircon U–Pb age of 478 ± 3 Ma (Zhu and Xu, 2006).

Plutons occurred in the northern West Junggar Region includes the Late Silurian–Early Devonian (ca. 422 to 405 Ma, Chen et al., 2010), the Early Carboniferous (ca. 346 to 321 Ma, Han et al., 2006; Zhou et al., 2008) and latest Late Carboniferous–Middle Permian (ca. 304 to 263 Ma, Han et al., 2006; Zhou et al., 2008) granitoids based on SHRIMP and LAICP-MS zircon U–Pb ages. The Late Silurian–Early Devonian granitoids mainly occur in the Ximisitai Mountains, the Early Carboniferous granitoids in the Tarbgatay and Saur Mountains and the latest Late Carboniferous–Middle Permian in the Wuerkashier, Tarbgatay, and Saur Mountains.

The Xiemisitai Mountains is bounded by two major faults, the northern Hongguleleng fault and the southern Xiemisitai fault (Fig. 2). Volcanic activity in the Xiemisitai Mountains occurred during the Middle Devonian to Early Carboniferous (BGMRXUAR, 1993). The Hujiersite Group of Middle Devonian, the oldest Group in the Xiemisitai Mountains, consists of a series of intermediate to felsic volcanic and pyroclastic rocks. The Zulumute Group of Upper Devonian and Hebukehe Group of Early Carboniferous contain volcanic rocks and sedimentary rocks. Our studies focused on the Middle Devonian Hujiersite Group in the east part of the Xiemisitai Mountains (Fig. 2). The plutons of the Late Silurian–Early Devonian (Chen et al., 2010) occurred in the Xiemisitai Mountains include gabbro, diorite, and monzonitic and K-feldspar granites. The regional structure is characterized by a series of approximately EW-trending faults including the Hongguleleng and Xiemisitai faults, although NE-, and NW-trending structures are also present (Fig. 2).

3. Xiemisitai rocks

3.1. Field mapping

We have mapped volcanic rocks and their subvolcanic units over 20 km^2 of the Xiemisitai Mountains (Fig. 3). Based on mineralogical composition and geochemical data (see below), the

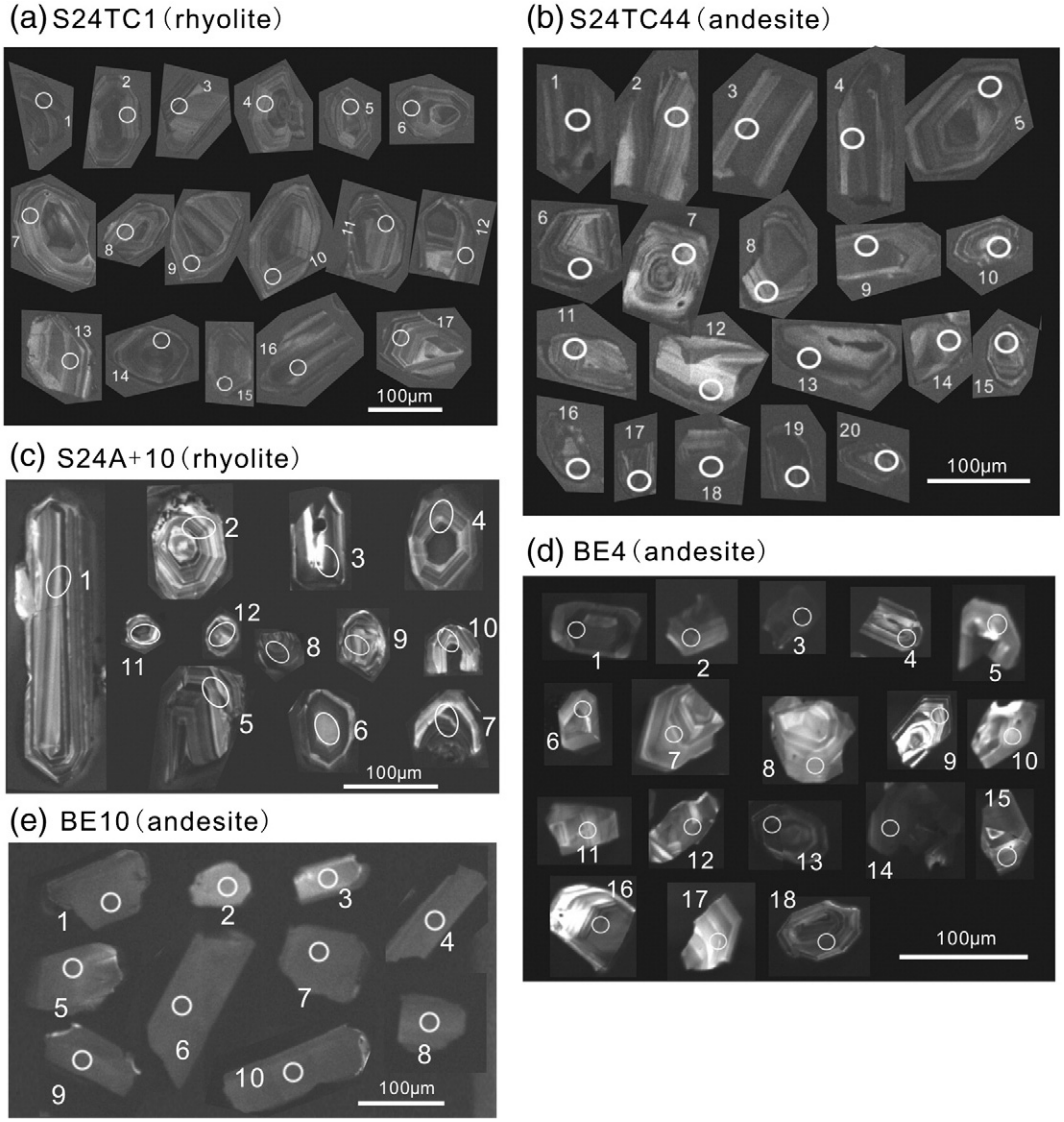

Fig. 4. SEM cathodoluminescence (CL) images of sectioned zircon grains from the Xiemisitai volcanic rocks from the east section (a, b, c) and west section (d, e) of the Ximisitai Mountains. Circle and numbered spots indicate the locations of SISM analysis with the measured age in Ma.

investigated volcanic rocks include Middle Devonian andesite, rhyolite and their pyroclastic equivalents. The andesite and rhyolite are widespread in the study area and form moderately high mountaneous rigdes, and associated pyroclastic rocks (volcanic breccia and minor tuff) are scattered in the study area (Fig. 3). The Xiemisitai subvolcanic units include Middle Devonian felsite, granite-porphyry, diabase and diorite-porphyry. Clear intrusive contacts are observed between the subvolcanic units and surrounding volcanic rocks and show an important evolution of magmatic activities from volcanic eruption to subvolcanic intrusion (Fig. 3). The felsite is widespread in the study area and form high mountains. The granite-porphyry stock (volcanic neck) forms a 1 km^2 wide circular depression in the center area (Fig. 3). Some diabase and diorite-porphyry dykes intrude along faults.

A granite mass cropped out in the northeastern part (Fig. 3) with the zircon U–Pb age of 414 ± 5 Ma, Early Devonian (Chen et al., 2010).

3.2. Petrography

3.2.1. The volcanic rocks

The andesites show slight flow structure defined by the parallel arrangement of the plagioclase phenocrysts. They contain about 20–25 modal percent phenocrysts of plagioclase (An_{40-50}), hornblende, and biotite in a hyalopilitic matrix dominated by plagioclase.

The pyroclastic rocks represented by andesitic volcanic breccias and andesitic crystal-lithic tuffs. The andesitic volcanic breccias are formed by angular to subrounded andesite fragments (up to 2–5 mm across up, most aboundant) and boulders (up to 30 mm long) embedded in a fine-grained andesitic tuffaceous matrix. Crystal-vitric tuff is andisitic in composition, and contains rock fragments (up to 2 mm across), vitric fragments (up to 0.3 mm across) and crystal fragments (up to 0.2 mm long) of plagioclase and hornblende set in a tuffaceous andesitic matrix.

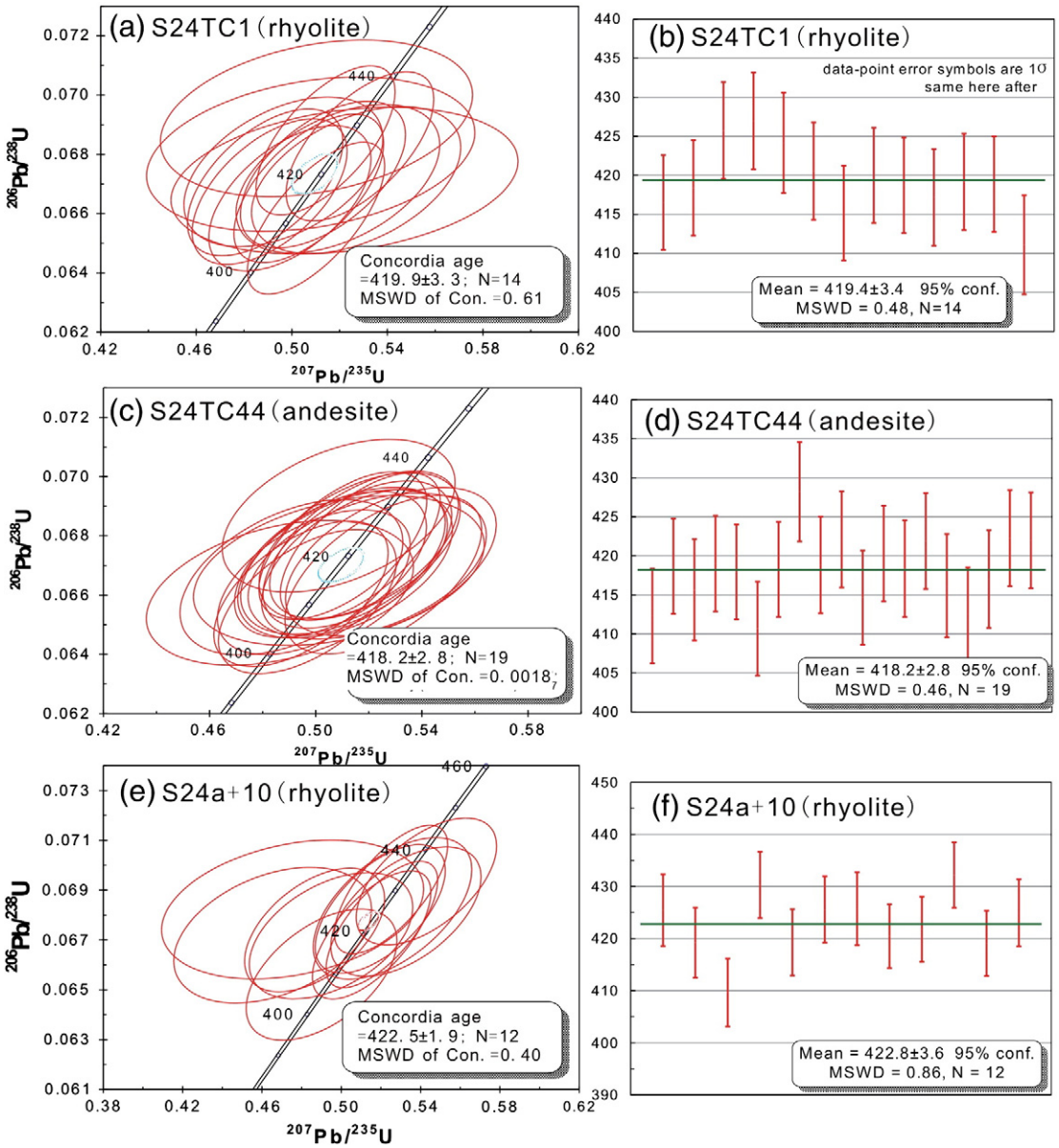

Fig. 5. Concordia and the weighted mean plots of SISM U–Pb isotopic analyses of zircon from the Xiemisitai volcanic rocks in the east section (a–f) and west section (g–j) of the Ximisitai Mountains.

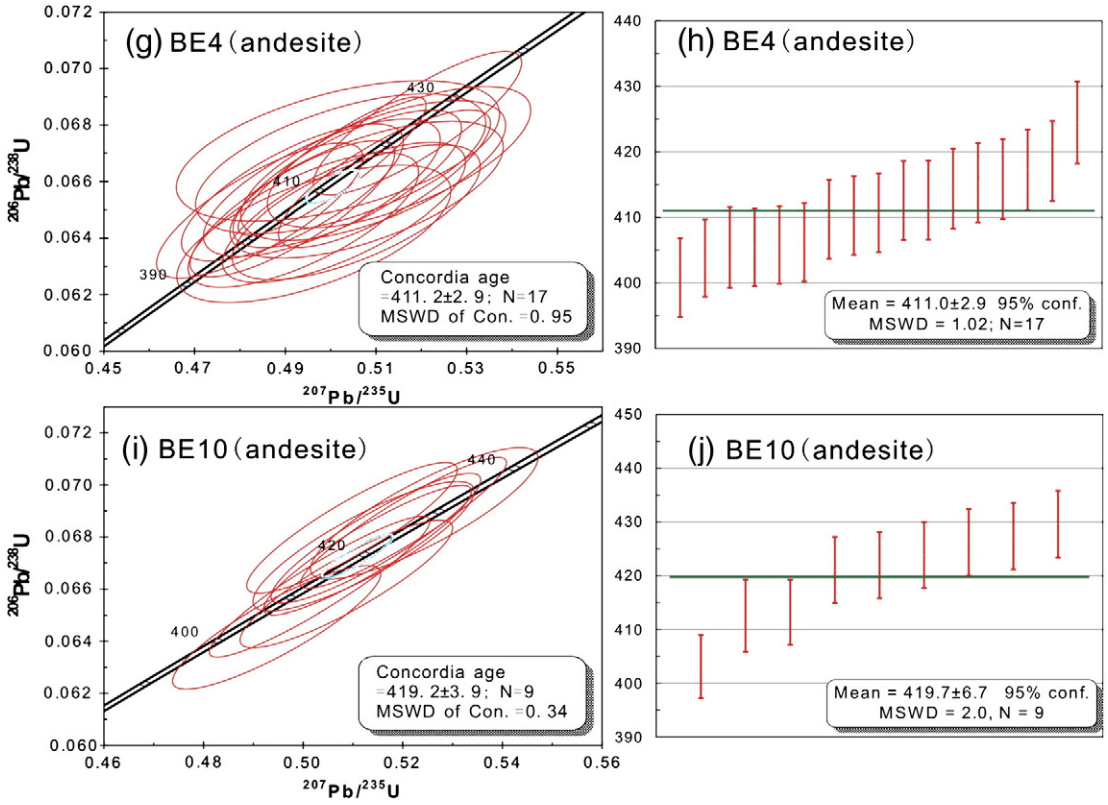

Fig. 5 (*continued*).

The rhyolites exhibited the markedly flow lines with a conspicuous porphyritic texture in which medium-grained plagioclase feldspar ($An_{10–20}$) phenocrysts and some biotite occur in a microgranular to vitrophyric groundmass. The main constituent minerals of the groundmass are quartz, plagioclase feldspar and K-feldspar. The rhyolitic volcanic breccias consist of rhyolite fragments (from 2 mm across up to 20 mm long) cemented by a felsic matrix.

3.2.2. Subvolcanic rocks

The hypabyssal rocks occurred in the studied area include felsites, granite-porphyry stock and diabase and diorite-porphyry dykes. The felsites have a fine-grained felsitic texture with obvious grain boundary and are similar to the Xiemisitai rhyolites in composition. They consist of microcrystalline quartz, plagioclase feldspar and minor K-feldspar. The granite porphyry is texturally porphyritic. The phenocrysts are coarse-grained plagioclase (up to 0.5–1 mm across) and the groundmass is micro-granitic texture consisting of quartz, plagioclase and K-feldspar. The diabases contain plagioclase, augite and hornblende. They are poikilophitic texture which coarse-grained augite and hornblende include fine-grained plagioclase. The diorite porphyry is porphyritic texture. The phenocrysts are plagioclase, hornblende and biotite and the groundmass contains plagioclase, quartz, and rare magnetite.

4. Methods and results

4.1. Analytical methods

The forty-two representative fresh volcanic rocks and subvolcanic units in the Xiemisitai Mountains were petrographically selected for chemical analyses. They are andesite, rhyolite, felsite and granite porphyry (Fig. 3). From all these, six volcanic rock and four subvolcanic units samples were selected for Rb, Sr, Sm, Nd and Pb isotope compositions analyses. Beside that, five volcanic rocks were selected for SIMS zircon U–Pb ages. All samples were measured at the Institute of Geology and Geophysics, Chinese Academy of Sciences, Beijing.

About 0.5–1.0 kg of each sample was crushed and quartered. A 100-g sample was milled and analyzed for major oxides, rare earth elements (REE), selected trace elements and Rb, Sr, Sm, Nd and Pb isotope compositions. Major elements were analyzed using a XRF-1500 Sequential X-ray Fluorescence Spectrometry on fused glass beads, with FeO and loss-on-ignition were analyzed by wet chemical methods. Analytical precision based on certified standards and duplicate analyses are expressed in terms of relative percentages, which range from ±1% to ±2%. An inductively Coupled Plasma Mass Spectrometer (ICP-MS) was used to analyze trace elements and REE. 100-g of sample was digested in beakers using a hot $HF + HNO_3$ mixture followed by a $HF + HNO_3 + HClO_3$ mixture to ensure complete dissolution and then taken up in 1% HNO_3 (dilution factor of >2000). The measurement error and drift were controlled by regular analysis of standard samples with a periodicity of 10%. Analyzed uncertainties of ICP-MS data at the ppm level are better than 10%.

Rb, Sr, Sm and Nd isotope compositions were analyzed using a MAT-262 with the analytical procedures similar to those described by Chen et al. (2002). Procedural blanks were <100 pg for Sm and Nd and <50 pg for Rb and Sr. The $^{87}Sr/^{86}Sr$ ratios were normalized to $^{86}Sr/^{88}Sr = 0.1194$ and the $^{143}Nd/^{144}Nd$ ratios to $^{146}Nd/^{144}Nd = 0.7219$. Typical within-run precision (2σ) was ±0.000010 and ±0.000013 for Sr and Nd isotopic ratios, respectively. The measured values for the JMC Nd standard and NBS987 Sr standard were $^{143}Nd/^{144}Nd = 0.511937 \pm 7$ (2σ, n = 12) and $^{86}Sr/^{88}Sr = 0.710226 \pm 12$ (2σ, n = 12), respectively, during the period of data acquisition. Pb isotopic ratios were analyzed with the same mass spectrometer; analytical precision is better than ±0.1‰.

Samples for U–Pb zircon analysis were processed by conventional magnetic and density techniques to concentrate non-magnetic, heavy fractions. Zircon grains, together with zircon standard 91500 (1065 Ma, Wiedenbeck et al., 1995) were mounted in epoxy mounts

which were then polished to section the crystals in half for analysis. All zircons were documented with transmitted and reflected light micrographs as well as cathodoluminescence (CL) images to reveal their internal structures. The mount was vacuum-coated with high-purity gold prior to the secondary ion mass spectrometry (SIMS) analysis.

Measurements of U, Th and Pb were conducted using the Cameca IMS-1280 SIMS at the Institute of Geology and Geophysics, Chinese Academy of Sciences in Beijing. U–Th–Pb ratios and absolute abundances were determined relative to the standard zircon 91500 (Wiedenbeck et al., 1995), analyses of which were interspersed with those of unknown grains, using operating and data processing procedures similar to those described by Li et al. (2009). A long-term uncertainty of 1.5% (1 RSD) for $^{206}Pb/^{238}U$ measurements of the standard zircons was propagated to the unknowns (Li et al., 2010), despite that the measured $^{206}Pb/^{238}U$ error in a specific session is generally around 1% (1 RSD) or less. Measured compositions were corrected for common Pb using non-radiogenic ^{204}Pb. Corrections are sufficiently small to be insensitive to the choice of common Pb composition. An average present-day crustal composition (Stacey and Kramers, 1975) is used for the common Pb assuming that the common Pb is largely surface contamination introduced during sample preparation. Uncertainties on individual analyses in data tables are reported at a 1σ level; mean ages for pooled U/Pb (and Pb/Pb) analyses are quoted with 95% confidence interval. Data reduction was carried out using the Isoplot/Ex v. 2.49 program (Ludwig, 2001).

4.2. Results

4.2.1. Zircon U–Pb results

Five volcanic rocks from the Xiemisitai Mountains were chosen for age determinations. Their locations are shown in Figs. 2, 3. All measured zircons are transparent short euhedral prisms, which in many cases have well-developed oscillatory zoning without distinctively older cores and younger overgrowths in cathodoluminescence images (Fig. 4a–e). The zircon SIMS U–Pb dating results are presented in Appendix Table 1 and related concordant diagrams shown in Fig. 5a–j.

In the present work, most zircons are euhedral, transparent, and 50–300 μm in length with aspect ratios between 2:1 and 4:1. Euhedral concentric zoning is common in most crystals under cathodoluminescence images (Fig. 4). All zircons show Th/U ratios greater than 0.1 (Appendix Table 1), indicating a magmatic origin for the zircons. Common Pb is generally low; values for f_{206} (the proportion of common ^{206}Pb in total measured ^{206}Pb) are lower than 1% for most analyses. So the results of zircon U–Pb dating reported in the present work can constrain the precise age of the volcanic rocks in the Xiemisitai Mountains.

Fifteen analyses of 15 zircons in sample S24TC1(rhyolite) were obtained during a single analytical session (Appendix Table 1). Fourteen analyses are concordant in $^{206}Pb/^{238}U$ and $^{207}Pb/^{235}Pb$ within analytical errors (Fig. 5a), yielding a concordia age of 419.9 ± 3.3 Ma (MSWD of concordance = 0.61, 95% confidence interval; same hereafter, n = 14). This age is in agreement with the weighted mean $^{206}Pb/^{238}U$ age of 420.2 ± 3.2 Ma (Fig. 5b, MSWD = 0.69, n = 14), and can be interpreted as the best estimate of the crystallization age for sample S24TC1(rhyolite). The rejected analysis, spot 13 (Fig. 4a), may be a xenocrystal zircon, giving a $^{207}Pb/^{206}Pb$ age of 973.1 ± 13.6 Ma.

Nineteen analyses of 19 zircons from sample S24TC44 (andesite) were obtained during a single analytical session (Appendix Table 1). For 19 analyses, the ratios of $^{206}Pb/^{238}U$ and $^{207}Pb/^{235}Pb$ agree internally within analytical precision (Fig. 5c), and yielded a concordia age of 418.2 ± 2.8 Ma Ma (MSWD of concordance = 0.0018, n = 19). This age is identical to the weighted mean $^{206}Pb/^{238}U$ age of 418.2 ± 2.8 (Fig. 5d, MSWD = 0.46, n = 19), and can be interpreted as the best estimate of the crystallization age for sample S24TC44 (andesite).

Twelve analyses from sample S24A + 10 (rhyolite) were performed on 12 zircons in a single analytical session (Appendix Table 1). All U–Pb results are concordant within error (Fig. 5e). A concordia age is calculated at 422.5 ± 1.9 Ma (MSWD of concordance = 0.40, n = 12). This age is in agreement with the weighted mean $^{206}Pb/^{238}U$ age of 422.8 ± 3.6 Ma (Fig. 5f, MSWD = 0.86, n = 12), which is considered as the best estimate for the crystallization age of sample S24A + 10 (rhyolite).

Seventeen analyses of 17 zircons from sample BE4 (andesite) were obtained (Appendix Table 1). All the analyses are concordant in $^{206}Pb/^{238}U$ and $^{207}Pb/^{235}Pb$ within analytical errors (Fig. 5g). They yield a concordia age of 411.2 ± 2.9 Ma (MSWD of concordance = 0.95, n = 17). This age is in good agreement with the weighted mean $^{206}Pb/^{238}U$ age of 411.0 ± 2.9 Ma (Fig. 5h, MSWD = 1.02, n = 17), which is considered the best estimate for the crystallization age of sample BE4 (andesite).

Ten analyses of 10 zircons in sample BE10 (andesite) were obtained during a single analytical session (Appendix Table 1). Nine analyses are concordant in $^{206}Pb/^{238}U$ and $^{207}Pb/^{235}Pb$ within analytical errors (Fig. 5h), yielding a concordia age of 419.2 ± 3.9 Ma (MSWD of concordance = 0.34, n = 9). This age is in agreement with the weighted mean of 419.7 ± 6.7 Ma (Fig. 5i, MSWD = 2.0, n = 9), which is interpreted as the estimate of the crystallization age for sample BE10 (andesite). The rejected analysis, spot 1, may be a xenocryst, giving a $^{206}Pb/^{238}U$ age of 765.6 ± 10.8 Ma.

Three samples (S24TC1, S24TC44 and S24A + 10) from the east part of the Xiemisitai Mountains (Fig. 3) give indistinguishable crystallization ages within analytical errors, averaging at ca. 420 Ma. All

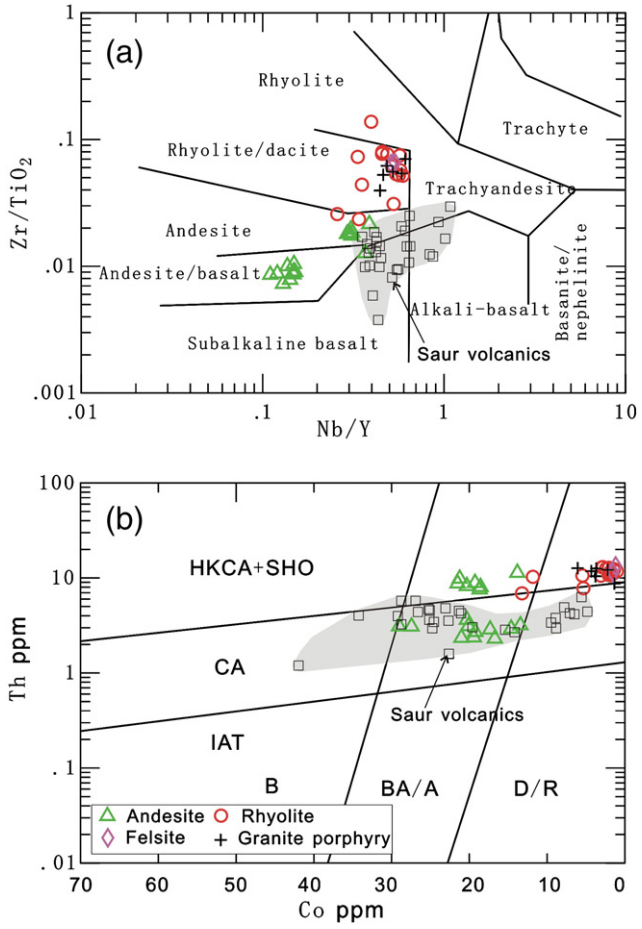

Fig. 6. (a) Zr/TiO_2 vs. Nb/Y (Winchester and Floyd, 1977), (b) Th vs. Co (Hastie et al., 2007) discrimination diagrams of the analyzed samples showing geochemical classification of the Xiemisitai volcanic rocks and their subvolcanic rocks. The respective fields of the Saur volcanic rocks (Shen et al., 2008a) are shaded. CA, medium-potassium calc-alkaline series; HKCA, high-potassium calc-alkaline series. IAT, island arc tholeiite; SHO, shoshonite. B, basalt; BA/A, basaltic andesite and andesite; D/R, dacite and rhyolite (including latites and trachytes).

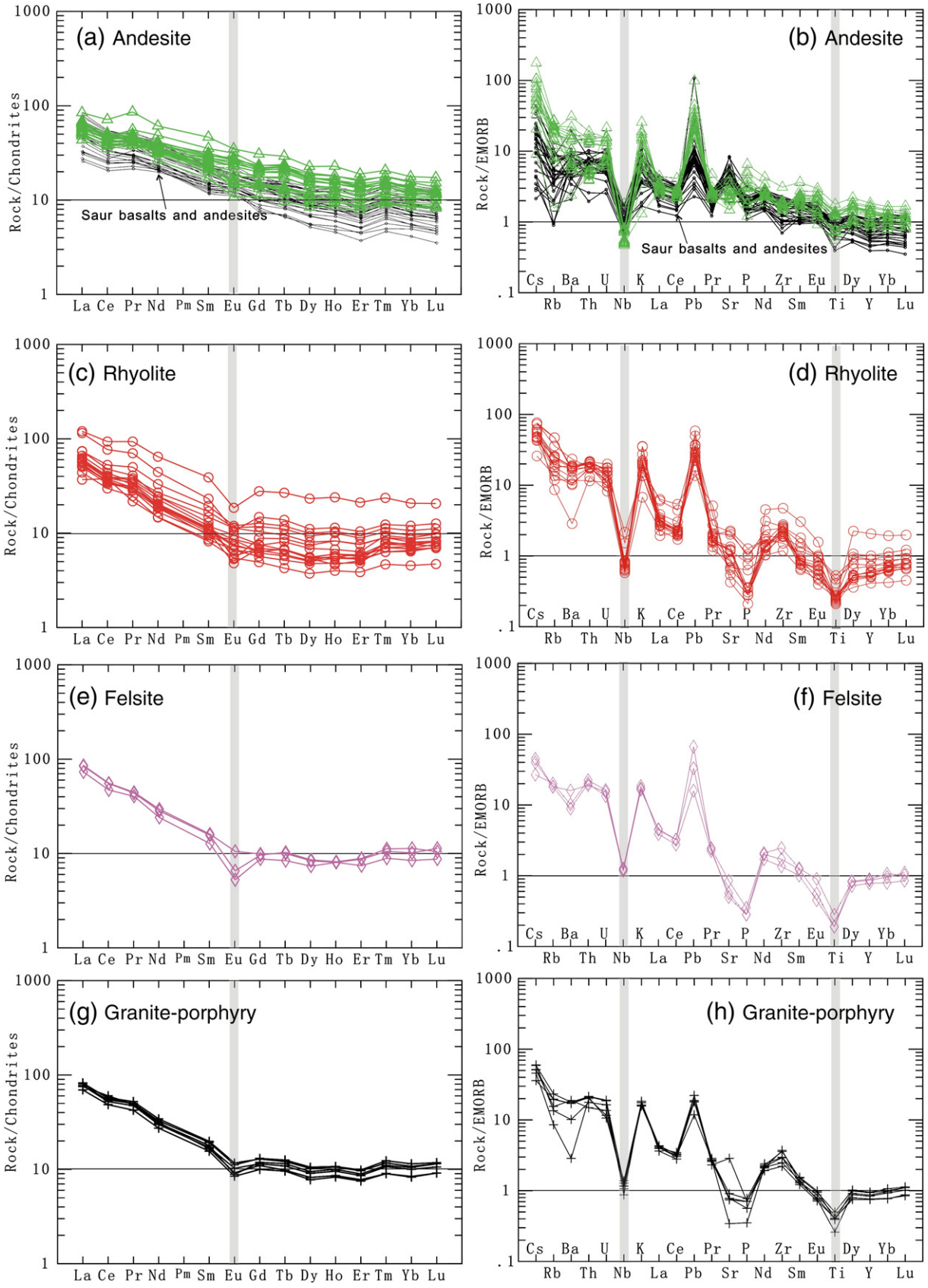

Fig. 7. Chondrite normalized (Nakamura, 1974) REE distribution and patterns of trace elements normalized (Sun and McDonough, 1989) to E-MORB for the Xiemisitai volcanic rocks in the Xiemisitai Mountains. The Saur volcanic rocks (Shen et al., 2008a) are also shown for comparison.

samples analyzed for Sr–Nd–Pb isotopes are selected from this area. We, therefore, calculated initial $^{87}Sr/^{86}Sr$, $^{143}Nd/^{144}Nd$, $^{206}Pb/^{204}Pb$, $^{207}Pb/^{204}Pb$, $^{208}Pb/^{204}Pb$ ratios of the Xiemisitai rocks at 420 Ma.

4.2.2. Major and trace elements

All samples analyzed in this study can be inferred that their results can reflect those of the fresh and most probably original magmatic rocks. Major and trace element concentrations of the studied volcanic rocks and their subvolcanic units are listed in the Appendix Table 2 and plotted in Figs. 6, 7, respectively. The results of the representative analyses are listed in Table 2.

The investigated volcanic rocks have a wide range of SiO_2 (53–77%) and high-potassium contents, whereas their subvolcanic units have a narrow range of SiO_2 (68–76%) and high-potassium contents (Table 2). Na, K and the low-field-strength elements are mostly mobile and susceptible to change during alteration (e.g., Humphris and Thompston, 1978), while the high-field-strength elements (such as Th, Ti, Zr, Y, Nb, Ta, and Hf) and the REE are essentially immobile during all but the most severe seafloor-hydrothermal alteration (e.g., Pearce, 1975; Wood et al., 1979) and the high-salinity, oxidized fluid–rock interaction at temperatures >400 °C (Dongen et al., 2010). Thus, only immobile elements such as the high-field-strength elements and REE are used in the discussion on classification and petrogenesis of these rocks. In the Zr/TiO_2 versus Nb/Y diagram, the samples plot in the andesite to rhyolite fields. In the Th versus Co diagram, the andesite samples plot mainly in the calc-alkaline (CA) series and high-potassium calc-alkaline (HKCA) series to shoshonite (SHO) series fields, whereas all rhyolite, felsite and granite porphyry samples plot mainly in the HKCA + SHO series fields.

Chondrite-normalized (Nakamura, 1974) REE patterns (Fig. 7) are marked by: (1) moderately LREE-enriched with weak negative Eu anomalies in andesites, and (2) enriched in LREE with moderate negative Eu anomalies in rhyolites, felsites and granite porphyries. Relative to enrich mid-ocean ridge basalts (E-MORB) (Sun and McDonough, 1989), the incompatible trace elements of the studied rocks (Fig. 7) show: (1) strong enrichment in the large ion lithophile elements (LILE) and with depletion in HFSE, Ti and Nb in andesites, and (2) strong enrichment in LILE and with more-depletion in HFSE, P, Ti and Nb in rhyolites, felsites and granite porphyries.

Comparison of the studied volcanic rocks with those of the Saur Mountains (Shen et al., 2008a) located in the north part of the

Table 2
Major and trace element data for volcanic rocks and their subvolcanic rocks from the Xiemisitai Mountains.

Sample	S12 + 51	S23 − 60	S23 + 210	S24 − 90	S24 − 5	XA − 1	XA − 2	XA − 5	XA − 3	GE + 280	GE + 360	XA − 6
Rock	A	R	A	R	A	R	R	R	F	GP	GP	GP
SiO_2	53.91	79.28	59.25	73.38	59.96	64.25	74.56	65.17	74.86	68.67	70.87	71.2
TiO_2	0.79	0.25	0.75	0.27	0.55	0.47	0.26	0.53	0.19	0.5	0.39	0.4
Al_2O_3	17.94	10.81	15.74	13.85	17.43	14.97	12.8	14.61	12.45	14.96	14.28	13.82
Fe_2O_3	4.64	1.27	5.21	1.46	2.94	2.95	1.18	3.07	1.03	1.37	1.28	1.19
FeO	2.62	0.37	1.89	0.2	2.3	1.57	0.18	1.66	0.16	1.03	0.66	0.69
MnO	0.12	0.01	0.12	0.03	0.14	0.11	0.02	0.12	0.03	0.09	0.09	0.04
MgO	3.38	0.14	2.84	0.14	2.23	2.34	0.22	1.46	0.32	0.69	0.49	0.66
CaO	4.68	0.22	4.48	0.6	4.13	3.62	0.36	3.52	0.97	1.39	1.55	0.9
Na_2O	2.29	3.27	3.28	4.45	3.17	3.99	3.58	4.33	4.22	4.98	4.56	4.8
K_2O	6.48	3.84	4.38	4.89	4.76	3.43	5.61	3.42	4.68	4.09	3.96	4.43
P_2O_5	0.26	0.03	0.25	0.04	0.17	0.18	0.04	0.15	0.04	0.11	0.08	0.1
Loi	2.64	0.46	1.82	0.38	1.7	1.46	0.56	1.5	1.08	1.66	1.78	1.18
Total	99.75	99.95	100.01	99.69	99.47	99.51	99.39	99.72	100.07	99.54	99.99	99.41
Li	31.27	36.26	16.41	4.86	33.6	25.51	5.10	27.44	6.02	9.28	6.74	14.31
Sc	22.79	7.25	25.15	2.7	14.5	13.7	2.71	16.83	2.50	5.32	4.53	3.75
V	201	11	183	10	85	130	15	126	12	38	21	22
Cr	100	184	119	166	64	13.33	2.73	4.99	6.03	72	150	4.90
Co	19.24	1.78	21.22	2.4	13.8	11.8	0.99	13.22	1.40	4.33	3.69	1.36
Ni	21.22	5.16	14.7	6.23	6.69	8.06	0.06	3.52	2.30	8.42	2.78	1.41
Ga	17.11	8.55	16.07	8.07	14.4	14.7	9.65	14.89	12.96	15.7	14.6	15.29
Rb	115	68	111	98	98	79	124	59	90	43	117	78
Sr	490	66	712	184	428	350	209	313	87.73	141	121	115
Y	22.49	45.31	21.36	11.81	16.5	16.18	12.95	19.75	17.20	21	20.6	16.84
Zr	142	345	137	141	1183	110	159	136	98.59	261	216	213
Nb	6.58	17.97	6.68	6.66	6.43	5.5	6.74	5.06	10.20	9.57	10.6	9.66
Cs	4.05	1.63	3.47	2.74	2.9	3	3.56	2.70	2.52	2.88	3.71	3.24
Ba	1242	577	954	970	1749	599	1043	670	506	163	1016	1075
La	19.28	39.74	22.71	20.03	22.2	19.37	18.17	18.71	24.41	25.5	26.6	27.20
Ce	42.18	80.77	44.22	35.15	38.0	33.96	29.82	34.03	41.24	47.1	49.5	48.98
Pr	5.34	10.47	5.61	3.69	4.52	4.09	3.44	4.26	4.57	5.61	5.85	5.50
Nd	21.39	40.73	21.9	12.2	16.5	15.46	11.89	16.94	15.36	20.6	21.6	19.83
Sm	4.57	7.91	4.75	2.19	3.44	3.01	2.08	3.45	2.62	3.91	4.02	3.35
Eu	1.16	1.43	1.24	0.56	0.83	0.87	0.36	0.88	0.41	0.86	0.9	0.71
Gd	3.87	7.67	4.15	1.82	3.02	2.86	1.89	3.24	2.44	3.6	3.55	3.03
Tb	0.64	1.26	0.64	0.28	0.46	0.45	0.30	0.51	0.40	0.59	0.57	0.45
Dy	4.1	7.98	3.88	1.76	2.89	2.75	1.91	3.19	2.55	3.62	3.51	2.81
Ho	0.87	1.68	0.8	0.4	0.6	0.58	0.41	0.69	0.57	0.75	0.74	0.59
Er	2.5	4.76	2.28	1.17	1.75	1.72	1.26	2.00	1.69	2.21	2.17	1.74
Tm	0.37	0.71	0.35	0.19	0.27	0.27	0.20	0.31	0.27	0.37	0.35	0.26
Yb	2.44	4.57	2.3	1.41	1.87	1.77	1.51	2.08	1.88	2.52	2.37	1.84
Lu	0.37	0.7	0.36	0.24	0.28	0.28	0.26	0.32	0.30	0.4	0.39	0.30
Hf	4.1	9.24	4.04	4.27	3.49	3.3	4.54	3.87	3.33	6.61	5.86	5.43
Ta	0.4	1.17	0.43	0.53	0.49	5.1	0.54	0.37	0.92	0.4	0.56	0.73
Tl	0.83	0.31	0.46	0.36	0.67	0.2	0.39	0.30	0.33	0.19	0.39	0.35
Pb	12.27	8.19	13.71	17.5	26.6	14.8	21.80	13.59	9.52	7.09	11.3	10.78
Th	8.87	10.7	9.82	12.5	11.3	10.3	11.82	6.92	12.09	12	12.8	8.93
U	2.86	2.76	2.78	2.51	2.78	3.2	3.12	1.96	2.40	2.09	3.34	2.44

Oxides in wt.%; trace elements in ppm. Abbreviations: A: andesite; R: rhyolite; F: felsite; GP: granite porphyry. LOI: loss on ignition.

Table 3
Nd–Sr–Pb isotopic data for the volcanic rocks and their subvolcanic rocks from the Xiemisitai Mountains.

Sample No.	S24−5	XA−1	XA−5	XA−2	S24−1	S12+51	XA−3	XA−6	GE1+280	GE1+360
Rock	A	R	R	R	R	R	F	GP	GP	GP
Rb		81.8	59.6	127.6				81.7	103.11	92.27
Sr		364	302.2	203.7				109.8	136.33	115.93
$^{87}Rb/^{86}Sr$		0.6502	0.5708	1.8146				2.1556	2.1907	2.3057
$(^{87}Sr/^{86}Sr)_m$		0.708251	0.70787	0.714635				0.715805	0.715439	0.716087
$2\sigma(\times10^{-6})$		15	14	10				12	12	11
$(^{87}Sr/^{86}Sr)_i$		0.704362	0.704456	0.70378				0.702911	0.702334	0.702294
Sm	3.42	2.9	2.97	1.98	1.62	4.83	2.58	3.19	3.68	3.57
Nd	16.93	14.36	13.72	10.93	8.26	23.01	14.47	17.99	18.99	18.69
$^{147}Sm/^{144}Nd$	0.122383	0.1223	0.1309	0.1097	0.1184	0.127224	0.1078	0.1072	0.117346	0.115831
$(^{143}Nd/^{144}Nd)_m$	0.512686	0.512718	0.512733	0.512654	0.512648	0.512704	0.512671	0.512731	0.512735	0.512715
$2\sigma(\times10^{-6})$	13	17	14	14	15	15	15	14	14	12
$(^{143}Nd/^{144}Nd)_i$	0.512349	0.512382	0.512373	0.512352	0.512322	0.512354	0.512374	0.512436	0.512412	0.512396
$\varepsilon Nd(t)$	0.93	1.56	1.85	0.31	0.19	1.28	0.64	1.81	1.88	1.49
T_{DM}	775	721	768	727	803	786	690	600	657	678
U		3.23	1.97	3.13	3.03		2.4	2.44		
Th		10.3	6.9	11.8	12.2		12.1	8.9		
Pb		14.8	13.6	21.8	25.3		9.5	10.8		
$(^{206}Pb/^{204}Pb)_m$		18.912±21	18.615±9	18.674±8	18.435±10		19.409±8	19.002±9		
$(^{207}Pb/^{204}Pb)_m$		15.602±25	15.535±9	15.588±8	15.570±9		15.605±8	15.554±9		
$(^{208}Pb/^{204}Pb)_m$		38.766±33	38.361±9	38.657±9	38.412±10		39.213±8	38.658±8		
$(^{206}Pb/^{204}Pb)_i$		17.820	17.898	17.961	17.843		17.778	17.883		
$(^{207}Pb/^{204}Pb)_i$		15.541	15.491	15.547	15.537		15.539	15.549		
$(^{208}Pb/^{204}Pb)_i$		37.674	37.569	37.809	37.663		37.684	37.734		

Sm, Nd, Rb, Sr, U, Th and Pb in ppm. (m) is the measured value, (i) is the initial value, (t) is the idealized crystallization age. The $^{87}Sr/^{86}Sr$ ratios are normalized to $^{86}Sr/^{88}Sr=0.1194$ and the $^{143}Nd/^{144}Nd$ ratios to $^{146}Nd/^{144}Nd=0.7219$. $\varepsilon Nd(t)=[\{(^{143}Nd/^{144}Nd)_m/(^{143}Nd/^{144}Nd)_{CHUR}\}-1]10^4$, using $(^{143}Nd/^{144}Nd)_{CHUR}=0.512638$ (DePaolo, 1988). Initial (i) values calculated at 420 Ma. The model ages were calculated using a linear isotopic ratio growth equation: $t_{DM}=(1/\lambda)\ln\{1+[(^{143}Nd/^{144}Nd)_m-0.51315]/[(^{147}Sm/^{144}Nd)_m-0.2137]$ (0.51315 and 0.2137 from Miller and O'Nions, 1985). Decay constants used are 1.42×10^{-11} a^{-1} for ^{87}Rb, 6.54×10^{-12} a^{-1} for ^{147}Sm, for $^{238}U=1.55125\times10^{-10}$ a^{-1}, $^{235}U=9.8485\times10^{-10}$ a^{-1} and $^{232}Th=4.9475\times10^{-11}$ a^{-1} (Steiger and Jäger, 1977). Blank: not analyzed.

Xiemisitai Mountains (Fig. 2), shows that the herein studied Late Silurian–Early Devonian Xiemisitai volcanics are similar to the Early Carboniferous Saur volcanics except for enrichment in REE and incompatible trace elements from the former suite (Figs. 6, 7).

4.2.3. Sr–Nd–Pb isotopes

Ten samples from the Xiemisitai Mountains were chosen for Sr–Nd–Pb isotopes analyses. We obtained 6 Sr, 10 Nd and 6 Pb isotope ratios. Measured and initial (back-calculated to 420 Ma) isotopic ratios are reported in Table 3. The large-ion-lithophile elements (such as Rb and Sr) are susceptible to change during alteration (e.g., Humphris and Thompston, 1978), therefore, εSr(t) value of the samples may provide some significant reference. All samples show a limited range in their $^{143}Nd/^{144}Nd$ and $^{87}Sr/^{86}Sr$ ratios (Fig. 8a–d). Initial $^{87}Sr/^{86}Sr$ ratios of the Xiemisitai volcanic rocks are ranging from 0.70378 to 0.70445; their initial Nd isotopes display small variations between 0.512322 and 0.512382 and $\varepsilon_{Nd}(t)$ from +0.19 to +1.85. The Nd model ages T_{DM} are ranging between 803 and 721 Ma (Table 3). Initial $^{87}Sr/^{86}Sr$ ratios of the Xiemisitai subvolcanic units (felsite and granite porphyry) are from 0.702294 to 0.702911; their Nd isotopes range from 0.512671 to 0.512735, $\varepsilon_{Nd}(t)$ from +0.64 to +1.88. Their Nd model ages (T_{DM}) are more restricted varying between 690 and 600 Ma and are slightly younger than that of the Xiemisitai volcanic rocks (Table 3).

The Pb initial ratios of the Xiemisitai volcanic rocks are less variable ($^{206}Pb/^{204}Pb_i=17.82$–$17.96$, $^{207}Pb/^{204}Pb_i=15.49$–$15.54$, and $^{208}Pb/^{204}Pb_i=37.57$–$37.81$, Table 3, Fig. 8c–f). Initial Pb ratios of the Xiemisitai subvolcanic units share similar the Pb initial ratios, but are more less variable ($^{206}Pb/^{204}Pb_i=17.77$–$17.88$, $^{207}Pb/^{204}Pb_i=15.54$–$15.55$, and $^{208}Pb/^{204}Pb_i=37.68$–$37.73$, Table 3, Fig. 8c–f).

5. Discussion

The previous study suggest that the north West Junggar Region in China consists of an early Paleozoic (Ordovician–Silurian) island arc and two late Paleozoic (Devonian–Carboniferous) island arcs (He et al., 2004; Wang, 1996). The former (Hongguleleng island arc) located in the center part, and the latter (Saur island arc and Xiemisitai island arc) located in the north (Saur Mountains) and south (Xiemisitai Mountains) sides of the former. Whereas, where the early Paleozoic volcanic arc occurred in West Junggar Region is controversial (He et al., 2004; Wang, 1996; Windley et al., 2007; Xiao et al., 2008). The petrogenesis of the early Paleozoic volcanic rocks and associated tectonic setting also needs further detailed studies. Moreover, all researchers suggested that the volcanic rocks in the Xiemisitai Mountains are Devonian–Carboniferous in age (BGMRXUAR, 1993; He et al., 2004; Wang, 1996; Windley et al., 2007; Xiao et al., 2008).

5.1. Ages of volcanic eruption

Previously, the volcanic rocks in the northern West Junggar Region were accepted to be the products of the Devonian–Permian volcanism and less related to deposition events during Ordovician and Silurian occurred in the Tarbahatay Mountains and Sharburti Mountains (BGMRXUAR, 1993). Our first Cameca SIMS zircon U–Pb isotope data (Figs. 2, 5), reveal that the volcanic rocks in the east fragment of Xiemisitai Mountains erupted at 422.5±1.9 Ma (rhyolite, sample S24A+10), 419.9±3.3 Ma (rhyolite, sample S24TC1) and 418.2±2.8 Ma (andesite, sample S24TC44), indicating that andesite and rhyolite magmas erupted nearly contemporaneously (Late Silurian), whereas the andesite magmas eruption in the west fragment of Xiemisitai Mountains ranges from 419.2±3.9 Ma (andesite, sample BE10) to 411.2±2.9 Ma (andesite, sample BE4) (Late Silurian–Early Devonian). Those new data, combined with mapping and petrologic studies, indicate that the Xiemisitai volcanic eruption focuses at Late Silurian–Early Devonian time rather than the Middle Devonian as previously published (BGMRXUAR, 1993). The Xiemisitai volcanic rocks, therefore, belong to the Kekexionghuduke Group of the Late Silurian rather than the Hujiersite Group of the Middle Devonian defined previously in northern West Junggar Region (BGMRXUAR, 1993; Xinjiang Geological Bureau, 1979). These data represent the earliest arc-related magmatic event in the Xiemisitai Mountains. Granites in the Xiemisitai Mountains, dated by U–Pb SHRIMP and LA-ICP-MS range between 422 and 405 Ma (Chen et al., 2010), coeval age range with the Xiemisitai volcanic rocks. For this reason we

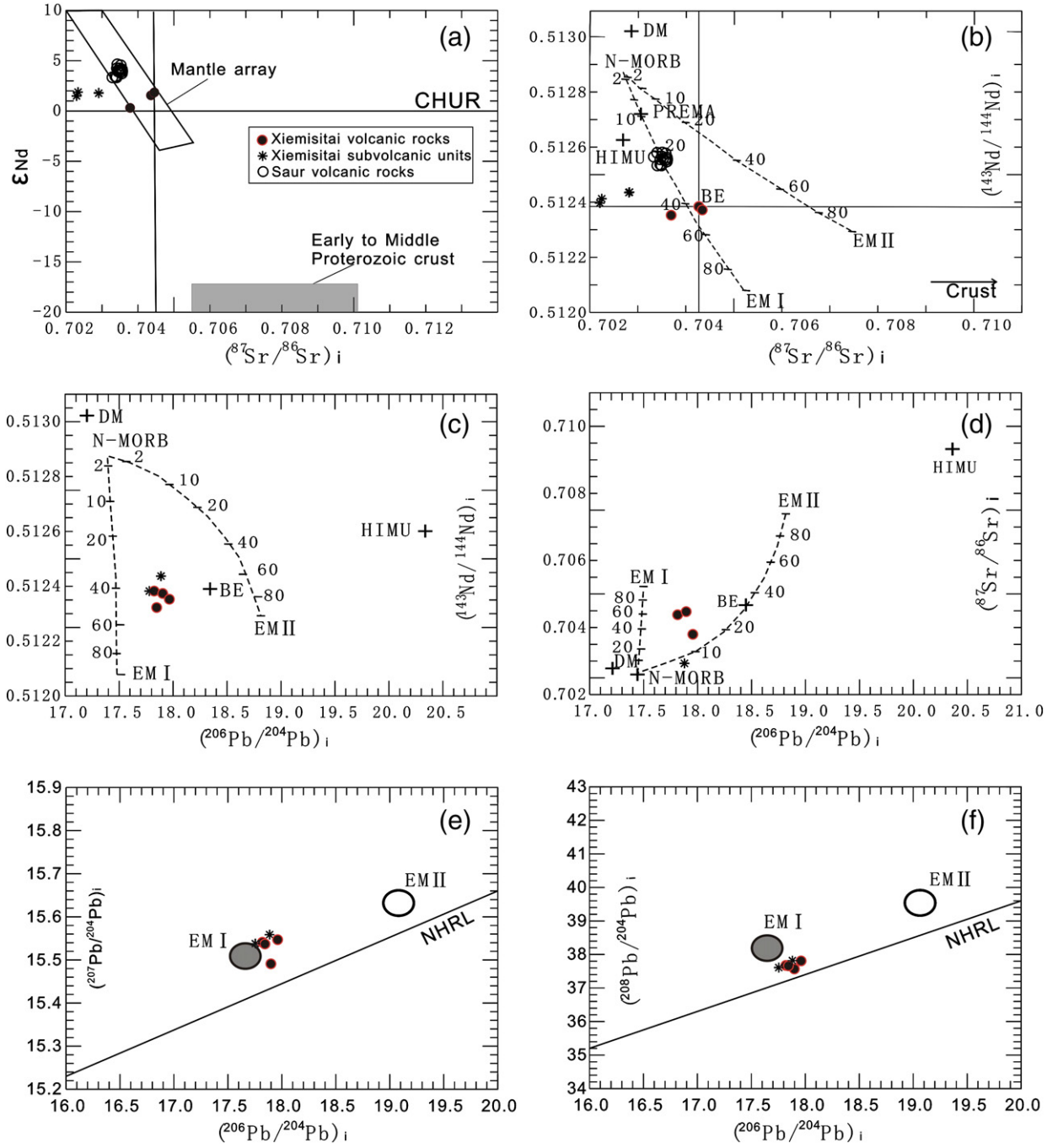

Fig. 8. Initial (420 Ma) isotope characteristics (After DePaolo, 1981; Alibert, 1985; Deckart et al., 2005; Karsli et al., 2007) of the Xiemisitai volcanic rocks and their subvolcanic units from this work and the Saur volcanic rocks from our previous work (Shen et al., 2008a). (a) εNd(t) vs. $(^{87}Sr/^{86}Sr)_i$ diagram (the early to middle Proterozoic crust from Hu et al., 2000). (b) $(^{143}Nd/^{144}Nd)_i$ versus $(^{87}Sr/^{86}Sr)_i$, (c) $(^{143}Nd/^{144}Nd)_i$ versus $(^{206}Pb/^{204}Pb)_i$, (d) $(^{87}Sr/^{86}Sr)_i$ versus $(^{206}Pb/^{204}Pb)_i$, (e) $(^{207}Pb/^{204}Pb)_i$ versus $(^{206}Pb/^{204}Pb)_i$, and (f) $(^{208}Pb/^{204}Pb)_i$ versus $(^{206}Pb/^{204}Pb)_i$. The diagram shows mixing lines with percentages of mixing between N-MORB and EMI or EMII end-members. DM, depleted mantle; BSE, bulk silicate Earth; EM1 and EM2, enriched mantle; HIMU, mantle with high U/Pb ratio.

suggest that the Late Silurian–Early Devonian is an important period of volcanic eruption and granite emplacement in the northern West Junggar Region. It is possible that a suite of volcano strata may continuously extend from the Sharburti Mountains in the east through Xiemisitai Mountains to the southern slope of the Tarbgatay Mountains close to the border of China–Kazakhstan, which are dominated by the Silurian strata, with Ordovician, Devonian and Carboniferous ones, and may be correlated with those counterparts in East Kazakhstan.

It is supported by their volcanic rock association and evolution occurred in East Kazakhstan and China. A peculiar feature of the Boshchekul–Chingiz volcanic suite in East Kazakhstan is the overwhelming dominance of andesite, with only minor occurrences of acid volcanics in the Late Cambrian to Early Silurian (Windley et al., 2007; Yakubchuk and Degtyarev, 1998). Moreover, the Boshchekul–Chingiz magmatic rocks belong to calc-alkalic (CA) series and shoshonite–latite series (Korobkin and Buslov, 2011). The volcanic suite in the Tarbgatay and Sharburti Mountains in China is characterized by andesite and basaltic andesite in Middle Ordovician (BGMRXUAR, 1993), similar to the Boshchekul–Chingiz volcanic suite. The volcanic suite in the Xiemisitai Mountains in China contains CA and high-potassium calc-alkaline (HKCA) series andesite and shoshonite

(SHO) + HKCA series ryholite in Late Silurian–Early Devonian (Fig. 6a, b). It indicates an evolved magmatic activity from dominant mafic magmatic activity to mafic and felsic magmatic activity from Ordovician to Silurian. Therefore, it is possible that the Cambrian to Silurian Boshchekul–Chingiz volcanic suite in East Kazakhstan extends eastward to the northern West Junggar Region of China, from the southern slope of the Tarbgatay Mountains through the Xiemisitai Mountains to the Sharburti Mountains.

5.2. Petrogenesis

The Xiemisitai andesites are plot in the andesite/basalt fields and range from CA series to HKCA + SHO series (Fig. 6a, b). They are enriched in LREE compared with typical E-MORB (Fig. 7a), but they are significantly depleted in Nb and Ti (Fig. 7b). Their Nb/Yb ratios range between that of N-MORB and OIB, in contrast to their Th/Yb ratios, which are much higher than that of the mantle array (Fig. 10). The Xiemisitai rhyolites, felsites and granite porphyries are plot in the rhyolite/dacite fields and are HKCA + SHO series (Fig. 6a, b). They have enriched LREE and also have large negative Nb and Ti anomalies (Fig. 7), an enrichment of Th/Yb compared to the mantle array (Fig. 10) and a calc-alkaline signature (Fig. 11). Their Nb/Yb ratios range between that of E-MORB and OIB. In a Th–Ta–Hf/3 and Y/15–La/10–Nb/8 diagrams (Fig. 11), all samples plot in the island arc calc-alkaline basalts field. These suggest that they formed in an island arc setting and were derived from a mantle wedge contaminated by subducted material (e.g., Kay, 1984; Münker et al., 2004).

Based on Nd–Sr–Pb isotope systematics, the sources of the Xiemisitai volcanic rocks and their subvolcanic units can be further limited. The Xiemisitai volcanic rocks plot in the "mantle array" (Fig. 8a), in detail, they lie on a mixing line between N-MORB and EMI component, close to the so-called BSE (Bulk Silicate Earth), while the Xiemisitai subvolcanic units are displaced to the left side of the "mantle array" and mixing line (Fig. 8a, b) with similar εNd(t) value to the Xiemisitai volcanic rocks. The positive εNd(t) value of the Xiemisitai volcanic rocks and their subvolcanic units is indicative of mantle contribution in an island arc setting, while a lower εSr(t) value of the Xiemisitai subvolcanic units may imply weakly hydrothermal alteration after the formation of the granite stock.

The eruption of the Xiemisitai volcanic rocks is earlier than the emplacement of the Xiemisitai subvolcanic units based on their occurrence, but very small differences in εNd(t) values (Table 3) between the volcanic rocks (+0.19 to +1.85) and their subvolcanic rocks (+0.64 to +1.88) reflect their isotopic homogenization in magma source or their co-source. Modeling using the Sr, Nd and Pb isotopic composition indicates that all samples can be explained by mixing between about 50 wt.% of melts with N-MORB characteristics and 50 wt.% of sedimentary end-member, isotopic similar to EMI (Fig. 8b–d). Lead isotopic ratios of the samples also indicate an EMI source (Fig. 8e, f) that can be considered as an end-member of the mixing process in the genesis. Probably, the Xiemisitai volcanic rocks and their subvolcanic units derived from a mantle wedge with significant mixing of subducted EMI in a subduction zone.

The lower positive εNd(t) value corresponding Nd mean crustal residence ages in the range of 600–803 Ma for Xiemisitai samples indicate significant involvement of Neoproterozoic primitive crust in the formation of the Xiemisitai magmatic arc (Fig. 9). It is supported by zircon U–Pb dating results of the volcanic rocks that two old ages of 973.1 ± 13.6 Ma and 765.6 ± 10.8 Ma (Precambrian age) occurred in Samples S24TC1 and BE10 (Appendix Table 1).

Comparison of the studied volcanic rocks with the volcanic rocks of the Saur Mountains, using published data from Shen et al. (2008a), shows that the Early Carboniferous Saur volcanic rocks derived from a depleted mantle source with minor mixing of subducted EMI (Fig. 8a, b). The isotopic signature of the Saur rocks ($\varepsilon_{Nd}(340) = +3.5$ to $+4.8$; $I_{Sr} = 0.70335$ to 0.70362, Shen et al., 2008a) and the corresponding Nd model ages (600 to 610 Ma) support a significant involvement of Neoproterozoic primitive crust in the formation of the Saur magmatic arc (Fig. 9).

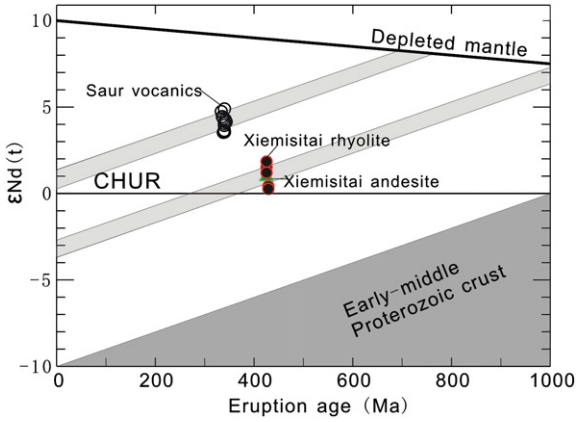

Fig. 9. Nd isotopic evolution and Nd isotope data of the Xiemisitai and Saur volcanic rocks. The early to middle Proterozoic crust is from Hu et al. (2000).

5.3. Tectonic implications

The early Paleozoic volcanic rocks exclusively crop out in the Boshchekul–Chingiz volcanic arc and the late Paleozoic volcanic rocks are confined to the Zharma–Saur volcanic arc, giving rise to two parallel EW-trending magmatic belts in northern West Junggar Region and adjacent East Kazakhstan (Figs. 1b, 2). In China, they are separated by an EW-trending Hongguleleng ophiolite belt (Fig. 2, Chen et al., 2010; IGCAGS, 2006; Zhu and Xu, 2006). In East Kazakhstan, they are separated by an NW-trending West Tarbgatay ophiolite belt (Fig. 2, Yakubchuk and Degtyarev, 1998; Zhu and Xu, 2006). The Boshchekul–Chingiz volcanic arc in China is separated by the EW striking Xiemisitai fault through the south of the Xiemisitai and Sharburti Mountains from the southern West Junggar accretionary complexes (Figs. 1, 2). The Late Paleozoic Zharma–Saur volcanic arc occupies the Tarbgatay and Saur Mountains of Kazakhstan and China (Fig. 2, Shen et al., 2008a; Zhu and Xu, 2006), and is separated by the Irtysh–Zaysan suture zone (Buslov et al., 2001, 2004; Windley et al., 2007).

5.3.1. Late Silurian–Early Devonian subduction setting

Late Silurian volcanic rocks have not been recognized in the Xiemisitai Mountains in previous studies. However, early Paleozoic (Cambrian to Silurian) volcanic rocks are widespread in Kazakhstan (Degtyarev et al., 2006; Korobkin and Smirnov, 2006; Kröner et al., 2008; Shatagin et al., 2001) and West Junggar Region in China (Sun et al., 2008; Wang et al., 2004). In Kazakhstan, the Boshchekul–Chingiz magmatic evolution began in the Early Cambrian and continued until the middle Early Silurian (Korobkin and Buslov, 2011). In China, Ordovician and Silurian strata occur widespread in the southern West Junggar Region and scatter in the Sharburti Mountains and in the Tarbgatay Mountains close to the border of China–Kazakhstan in the northern West Junggar Region (Fig. 2). A recent study confirms the presence of Late Silurian–Early Devonian granitoids in the West Junggar Region (Chen et al., 2010) and East Junggar Region (Guo et al., 2009). All these data indicate that early Paleozoic (Cambrian to Silurian) magmatism widely occurred in Northern Xinjiang and adjacent Kazakhstan. Therefore, it is possible that the Boshchekul–Chingiz volcanic arc extends eastward to the northern West Junggar Region of China.

The Xiemisitai volcanic rocks and their subvolcanic units are LREE-enriched, with a marked negative Nb anomaly and Th/Yb-enrichment. Their I_{Sr} values range from 0.702294 to 0.704456,

ε_{Nd}(420 Ma) from +0.19 to +1.88 with Nd model ages ranging between 600 and 803 Ma. Pb isotopic ratios ($^{206}Pb/^{204}Pb)_i$ are 17.77–17.96. One rhyolite (Sample S24TC1) and one andesite (Sample BE10) have the oldest ages of 973.1 ± 13.6 Ma and 765.6 ± 10.8 Ma, respectively (Appendix Table 1). Based on these characteristics, we infer that the investigated rocks formed in an island arc setting as indicated by a Th–Ta–Hf/3 and Y/15–La/10–Nb/8 diagrams (Fig. 11a). Therefore, the new data from the northern West Junggar Region, the Late Silurian–Early Devonian Xiemisitai volcanic rocks and their subvolcanic units, are subduction-related and probably contaminated by Neoproterozoic primitive crust and form part of the early Paleozoic (Cambrian to Silurian) Boshchekul–Chingiz volcanic arc. Meanwhile, accompanying with the Late Silurian–Early Devonian volcanism, copper mineralization widespread in the northern West Junggar Region, and formed the volcanic- and subvolcanic-related copper deposits and occurrences (Figs. 2, 3; Shen et al., 2010c). The late Silurian–Early Devonian volcanism is coeval with volcanic- and subvolcanic-related copper mineralization which occurrences are recognized in the Xiemisitai and Sharburti Mountains as well as the southern slope of the Tarbgatay Mountains. Therefore, the early Paleozoic Boshchekul–Chingiz metallogenic belt in East Kazakhstan may also extend to the northern West Junggaer Region in China which has potential implications for mineral exploration in this area.

5.3.2. Devonian–Early Carboniferous subduction setting

The late Paleozoic (Devonian–Carboniferous) Zharma–Saur volcanic arc occupies the Saur Mountains of Kazakhstan and China (Fig. 2). Based on our published data (Shen et al., 2008a), the Saur volcanic rocks, composed of calc-alkaline basalts and basaltic andesites (Fig. 7), are enriched in LILE with negative Nb and Ti anomaly (Fig. 7) and Th/Yb-enrichment (Fig. 10), all characteristic indicators of subduction, as indicated by a Th–Ta–Hf/3 and Y/15–La/10–Nb/8 diagrams (Fig. 11). They have low radiogenic Sr ($Sr_{(i)}$ = 0.70335–0.70362) and moderate radiogenic Nd (ε_{Nd} (340 Ma) = +3.5–+4.7). These characteristics suggest that these lavas were most likely products of a depleted mantle wedge from a subduction-related environment (Shen et al., 2008a).

The Irtysh–Zaysan Ocean between the Kazakhstan and Altai blocks presents during the Devonian and Early Carboniferous (Iwata et al., 1994, 1997), and thus the Zharma–Saur volcanic arc along the northeastern margin of the Kazakhstan block may be the product of southward subduction of the Irtysh–Zaysan Oceanic lithosphere (Didenko and Morozov, 1999; Vladimirov et al., 2008). The Devonian and Early Carboniferous volcanic rocks in the Saur Mountains are representative of arc magmatism caused by the southward subduction of the Irtysh–Zaysan Oceanic lithosphere beneath the northern West Junggar Region. The gold mineralisation developed in the Saur island

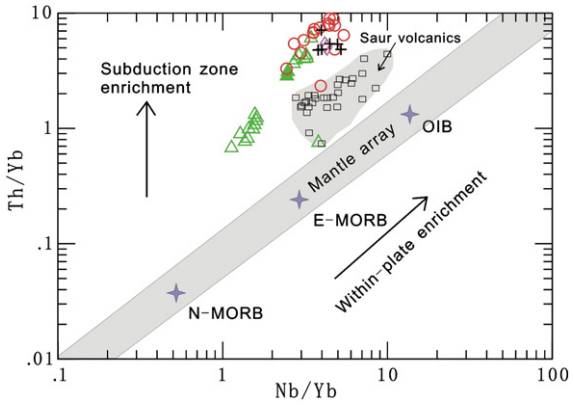

Fig. 10. Th/Yb–Ta/Yb diagram (Pearce and Peate, 1995; Sayit and Goncouglu, 2009) for the volcanic rocks in the Xiemisitai Mountains from this work and the Saur Mountains from our previous work (Shen et al., 2008a). Symbols are the same as in Fig. 6.

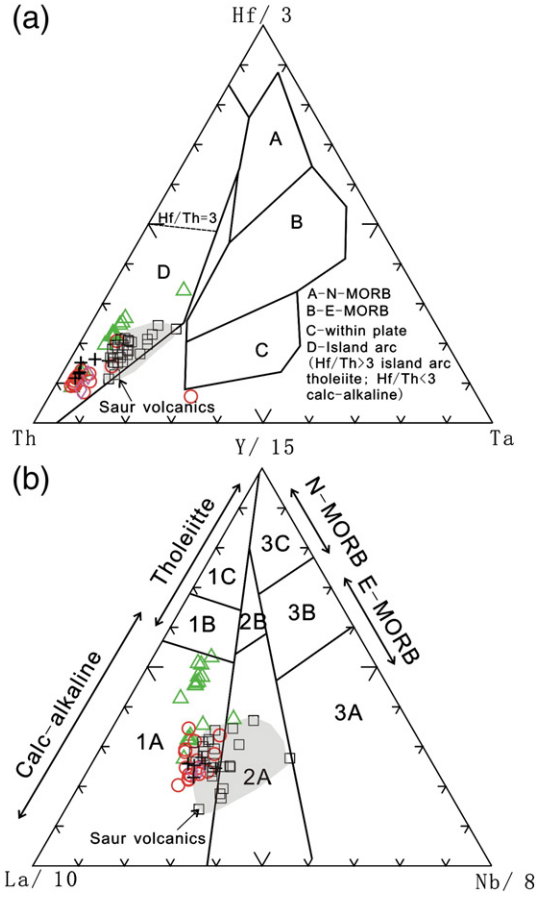

Fig. 11. Tectonic discrimination diagrams (a) Th–Ta–Hf/3 diagram (Wood, 1980) and (b) Y/15–La/10–Nb/8 diagram (Cabanis and Lecolle, 1989) for the Xiemisitai volcanic rocks (from this work) and Saur volcanic rocks (Shen et al., 2008a) from the northern West Junggar. Explanation: 1A = calcalkaline basalts, 1C = volcanic-arc tholeiites, 1B = overlap area between1A and 1C; 2A = continental basalts, 2B = backarc-basin basalts; 3A = alkali basalts; 3B = enriched MORB; 3C = depleted MORB. Symbols are the same as in Fig. 6.

arc and formed the volcanic-related gold deposits in the Zharma–Saur volcanic arc in China (Shen et al., 2007, 2008a; Zhou et al., 2008). The best examples are the Kuoerzhenkuola and Buerkesidai gold deposits. The ^{40}Ar–^{39}Ar ages of quartz fluid inclusions are 332.05 ± 2.02 Ma to 332.59 ± 0.51 Ma for the Kuoerzhenkuola deposit and 335.53 ± 0.32 Ma to 336.78 ± 0.50 Ma for Buerkesidai gold deposit, respectively (Shen et al., 2007). Therefore, the Zharma–Saur metallogenic belt in East Kazakhstan extends to the northern West Junggaer in China.

Based on above discussions and taking into consideration published data from adjacent areas, a simplified geodynamic evolution and associated mineralization for the study area can be divided into two periods: (1) Late Silurian–Early Devonian subduction period (422–411 Ma) (Fig. 12a): The southward subduction of the oceanic lithosphere forms the Boshchekul–Chingiz volcanic arc and associated copper mineralization; (2) Devonian–Early Carboniferous subduction period (380–334 Ma, Shen et al., 2008a; Zhou et al., 2008) (Fig. 12b): The southward subduction of the Irtysh–Zaysan Oceanic lithosphere forms the Zharma–Saur volcanic arc and associated gold mineralization.

This gives rise to two parallel EW- to NW-trending magmatic belts and associated metallogenic belts in the northern West Junggar Region and adjacent Kazakhstan (Figs. 1, 2), suggesting that the northern West Junggar Region is a part of the Kazakhstan block and that the Late Silurian–Early Devonian volcanic rocks and Devonian–Early Carboniferous volcanic rocks in the northern West Junggar Region are the constituents of the Boshchekul–Chingiz volcanic arc and Zharma–Saur volcanic arc, respectively. Therefore, the tectonic

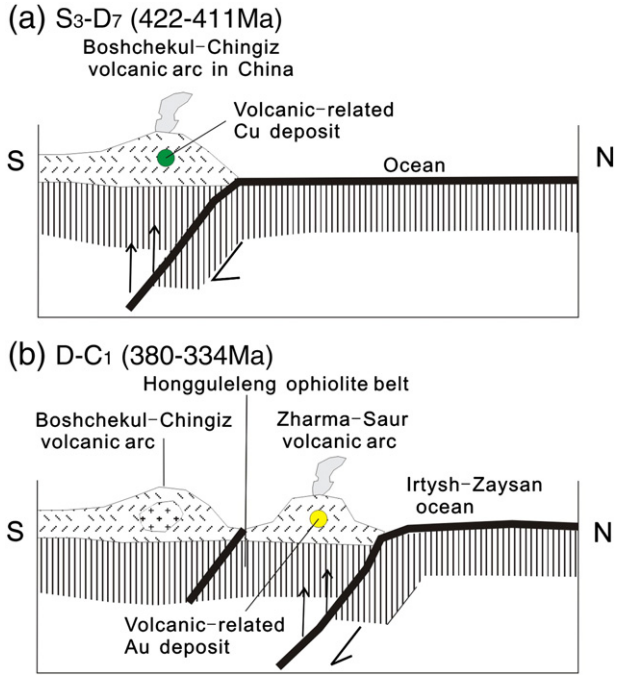

Fig. 12. Cartoon showing the evolution of geodynamic setting in the northern West Junggar Region, Xinjiang. (a) Production of Boshchekul–Chingiz island arc and associated copper mineralization responding to slab subduction in the Late Silurian–Early Devonian. (b) Production of Zharma–Saur island arc and associated gold mineralization responding to slab subduction in the Devonian–Early Carboniferous.

history of the northern West Junggar Region was characterized by accretion of arcs all created by southward subduction.

6. Conclusion

On the basis of SIMS zircon U–Pb ages, elemental and Nd–Sr–Pb isotopic data determined in this study, a Late Silurian–Early Devonian volcanic arc in northern West Junggar Region is recognized. It is probably the eastern extension of the Cambrian–Silurian Boshchekul–Chingiz volcanic arc of East Kazakhstan in China.

The Late Silurian–Early Devonian Xiemisitai volcanic rocks and their subvolcanic units are LREE-enriched, with a negative Nb anomaly and Th/Yb-enrichment, lower positive $\varepsilon_{Nd}(t)$ (+0.19 to +1.88) with corresponding Nd model ages (600 to 800 Ma), narrow range Pb isotopic ratios ($(^{206}Pb/^{204}Pb)_i = 17.77–17.96$). These new data indicate that the Xiemisitai rocks derived from a mantle wedge with significant mixing of subducted EMI in a subduction zone. They also indicate a significant involvement of Neoproterozoic primitive crust in the formation of the Xiemisitai magmatic arc. The formation of Devonian–Early Carboniferous Saur volcanic rocks, located in the north of the Xiemisitai Mountains, is similar to that of the Xiemisitai volcanic rocks. The southward subduction of the Oceanic lithosphere gives rise to two parallel volcanic arcs and associated metallogenic belts (Boshchekul–Chingiz and Zharma–Saur) in the northern West Junggar Region and adjacent Kazakhstan. The tectonic history of the northern West Junggar Region was characterized by accretion of two arcs all created by southward subduction.

Acknowledgments

We are very grateful to Wenjiao Xiao and Jingbin Wang for discussions, advice and improvements of the manuscript. Constructive comments by Katja Deckart and an anonymous reviewer and editor-in-chief Nelson Eby significantly improved the paper. Thanks are given to the members of the seventh Geology team, Zhejiang Geoexploration Bureau, for mapping in field. This paper was financially supported by the National Science Fund (Grant No. 40972064), Innovative Project of the Chinese Academy of Sciences (Grant No. KZCX2-YW-107) and National 305 Project (Grant No. 2011BAB06B01).

Appendix A. Supplementary data

Supplementary data to this article can be found online at doi:10.1016/j.lithos.2012.02.004.

References

Abdulin, A.A., Bespaev, H.A., Votsalevsky, E.S., Daukeev, S.Z.H., Miroshnichenko, L.A., 1996. Map of mineral resources of Kazakstan: Non-ferrous metals, Scale 1:2000000, IPC, Alma-Ata.
Abdulin, A.A., Esenov, ShE., 1975. Copper metallogenic belt of Kazakhstan, Izvestiya Academy of Science USSR. Series Geology 6, 1–14 (in Russian).
Alibert, C., 1985. A Sr–Nd isotope and REE study of late Triassic dolerites from the Pyrene'es (France) and the Messejana dyke (Spain and Portugal). Earth and Planetary Science Letters 73, 81–90.
BGMRXUAR (Bureau of Geology and Mineral Resources of Xinjiang Uygur Autonomous Region), 1993. Regional Geology of Xinjiang Uygur Autonomous Region. Geological Publishing House, Beijing. 841 pp. (in Chinese with English abstract).
Buslov, M.M., Saphonova, I.Yu., Watanabe, T., Obut, O.T., Fujiwara, Y., Iwata, K., Semakov, N.N., Sugai, Y., Smirnova, L.V., Kazansky, A.Y., 2001. Evolution of the Paleo-Asian Ocean (Altai-Sayan Region, Central Asia) and collision of possible Gondwana derived terranes with the southern marginal part of the Siberian continent. Geosciences Journal 5, 203–224.
Buslov, M.M., Watanabe, T., Fujiwara, Y., Iwata, K., Smirnova, L.V., Safonova, I.Yu., Semakov, N.N., Kiryanova, A.P., 2004. Late Paleozoic faults of the Altai region, Central Asia: tectonic pattern and model of formation. Journal of Asian Earth Sciences 23, 655–671.
Cabanis, B., Lecolle, M., 1989. La diagramme La/10–Y/15–Nb/8, Un outil pour la discrimination des series volcaniques et la mise en evidence des processes de melange et/ou de contamination crustale. Comptes Rendus de l Academie des Sciences Serie II 309, 2023–2029.
Chen, B., Arakawa, Y., 2005. Elemental and Nd–Sr isotopic geochemistry of granitoids from the West Junggar foldbelt (NW China), with implications for Phanerozoic continental growth. Geochimica et Cosmochimica Acta 69, 1307–1320.
Chen, F., Satir, M., Ji, J., Zhong, D., 2002. Nd–Sr–Pb isotopic composition of the Cenozoic volcanic rocks from western Yunnan, China: evidence for enriched mantle source. Journal of Asian Earth Science 21, 39–45.
Chen, J.F., Han, B.F., Jia, J.Q., Zhang, L., Xu, Z., He, G.Q., Wang, T., 2010. Zircon U–Pb ages and tectonic implications of Paleozoic plutons in northern West Junggar, North Xinjiang, China. Lithos 115, 137–152.
Deckart, K., Bertrand, H., Liégeois, J.P., 2005. Geochemistry and Sr, Nd, Pb isotopic composition of the Central Atlantic Magmatic Province (CAMP) in Guyana and Guinea. Lithos 82, 282–314.
Degtyarev, K.E., Shatagin, K.N., Kotov, A.B., Sal'nikova, E.B., Luchitskaya, M.V., Yakovleva, S.Z., Plotkina, Y.V., Fedoseenko, A.M., 2006. Early Paleozoic granitoids of theAqtau–Dzungar Microcontinent (Central Kazakhstan). Doklady Akademii Nauk 411, 80–84.
DePaolo, D.J., 1988. Neodymiun Isotope Geochemistry: an Introduction. Springer-Verlag, Berlin. 1~189.
DePaolo, D.J., 1981. Trace element and isotopic effects of combined wall-rock assimilation and fractional crystallization. Earth and Planetary Science Letters 53, 189–202.
Didenko, A.N., Morozov, O.L., 1999. Geology and paleomagnetism of Middle-Upper Paleozoic rocks of the Saur Ridge. Geotectonics 4, 64–80 (in Russian with English abstract).
Dongen, M.V., Weinberg, R.F., Tomkins, A.G., 2010. REE-Y, Ti, and P remobilization in magmatic rocks by hydrothermal alteration during Cu–Au deposit formation. Economic Geology 105, 763–776.
Guo, L.S., Zhang, R., Liu, Y.L., Xu, F.J., 2009. Zircon LA-ICP-MS U–Pb age of Tonghualing intermediate-acid intrusive rocks, Eastern Junggar, Xinjiang. Acta Scientiarom Naturalium Universitatis Pekinensis 45, 819–824.
Han, B.F., Ji, J.Q., Song, B., Chen, L.H., Zhang, L., 2006. Late Paleozoic vertical growth of continental crust around the Junggar Basin, Xinjiang, China (Part I): timing of post-collisional plutonism. Acta Petrologica Sinica 22, 1077–1086 (in Chinese with English abstract).
Hastie, A.R., Kerr, A.C., Pearce, J.A., Mitchell, S.F., 2007. Classification of altered volcanic island arc rocks using immobile trace elements: development of the Th–Co discrimination diagram. Journal of Petrology 48, 2341–2357.
He, G.Q., Chen, S.D., Xu, X., Li, J.Y., Hao, J., 2004. An introduction to tectonic map of Xinjiang and its neighboring area (1: 250 000). Geological Publishing House, Beijing. 65 pp.
Heinhorst, J., Lehmann, B., Ermolov, P., 2000. Paleozoic crustal growth and metallogeny of Central Asia: evidence from magmatic hydrothermal ore systems of Central Kazakhstan. Tectonophysics 328, 6–87.
Hu, A.Q., Jahn, B.M., Zhang, Y., 2000. Crustal evolution and Phanerozoic crustal growth in northern Xinjiang: Nd isotopic evidence. Part I. Isotopic characterization of basement rocks. Tectonophysics 328, 15–52.
Humphris, S.E., Thompston, G., 1978. Hydrothermal alteration of oceanic basalts by seawater. Geochimica et Cosmochimica Acta 42, 107–125.

IGCAGS (Institute of Geology of Chinese Academy of Geological Sciences), 2006. 1:2 500 000 Geological Map of the Western China and adjacent regions (4 sheets). Geological Publishing House, Beijing (in Chinese)
Iwata, K., Obut, O.T., Buslov, M.M., 1997. Devonian and Lower Carboniferous radiolarian from the Chara ophiolite belt, East Kazakhstan. News of Osaka Micropaleontologist 10, 27–32.
Iwata, K., Watanabe, T., Akiyama, M., Dobretsov, N.L., Belyaev, S.Y., 1994. Paleozoic microfossils from the Chara Belt (Eastern Kazakhstan). Russian Geology and Geophysics 35, 145–151 (in Russian).
Karsli, O., Chen, B., Aydin, F., Şen, C., 2007. Geochemical and Sr–Nd–Pb isotopic compositions of the Eocene Dölek and Sariçiçek Plutons, Eastern Turkey: implications for magma interaction in the genesis of high-K calc-alkaline granitoids in a post-collision extensional setting. Lithos 98, 67–96.
Kay, R.W., 1984. Elemental abundances relevant for identification of magma sources. Philosophical Transactions of the Royal Society of London A 310, 535–547.
Korobkin, V.V., Buslov, M.M., 2011. Tectonics and geodynamics of the western Central Asian Fold Belt (Kazakhstan Paleozoides). Russian Geology and Geophysics 52, 1600–1618.
Korobkin, V.V., Smirnov, A.V., 2006. Paleozoic tectonics and geodynamics of volcanic arcs in northern Kazakhstan. Russian Geology and Geophysics 47, 462–474.
Kröner, A., Hegner, E., Lehmann, B., Heinhorst, J., Wingate, M.T.D., Liu, D.Y., Ermelov, P., 2008. Paleozoic arc magmatism in the Central Asian Orogenic Belt of Kazakhstan: SHRIMP zircon ages and whole-rock Nd isotopic systematics. Journal of Asian Earth Science 32, 118–130.
Kudryavtsev, Y.K., 1996. The Cu–Mo deposits of Central Kazakhstan. In: Shatov, V., Seltmann, R., Kremenetsky, A., Lehmann, B., Popov, V., Ermolov, P. (Eds.), Granite-related Ore Deposits of Central Kazakhstan and Adjacent Areas. Glagol Publishing House, St. Petersburg. 119–144 pp.
Li, Q.L., Li, X.H., Liu, Y., Tang, G.Q., Yang, J.H., Zhu, W.G., 2010. Precise U–Pb and Pb–Pb dating of Phanerozoic baddeleyite by SIMS with oxygen flooding technique. Journal of Analytical Atomic Spectrometry 25, 1107–1113.
Li, X.H., Liu, Y., Li, Q.L., Guo, C.H., Chamberlain, K.R., 2009. Precise determination of Phanerozoic zircon Pb/Pb age by multi-collector SIMS without external standardization. Geochemistry, Geophysics, Geosystems 10, Q04010. doi:10.1029/2009GC002400.
Liu, G.R., Long, Z.N., Chen, Q.Z., Zhou, G., 2003. The formation age and geochemical characteristics of volcanic rock of Kuoerzhenkuolas gold mine in Xinjiang. Xinjiang Geology 21, 177–180 (in Chinese).
Ludwig, K.R., 2001. Users Manual for Isoplot/Ex rev. 2.49. Berkeley Geochronology Centre Special Publication. No. 1a, 56 pp.
Miller, R.G., O'Nions, R.K., 1985. Source of Precambrian chemical and clastic sediments. Nature 314 (325), 330.
Münker, C., Wörner, G., Yogodzinski, G., Churikova, T., 2004. Behaviour of high field strengths elements in subduction zones: constraints from Kamchatka–Aleutian arc lavas. Earth and Planetary Science Letters 224, 275–293.
Nakamura, N., 1974. Determination of REE, Ba, Mg, Na and K in carbonaceous and ordinary chondrites. Geochimica et Cosmochimica Acta 38, 757–773.
Pearce, J.A., 1975. Basalt geochemistry used to investigate past tectonic environments on Cyprus. Tectonophysics 25, 41–67.
Pearce, J.A., Peate, D.W., 1995. Tectonic implications of the composition of volcanic ARC magmas. Annual Review of Earth and Planetary Sciences 23, 251–285.
Sayit, K., Goncouglu, M.C., 2009. Geochemistry of mafic rocks of the Karakaya complex, Turkey: evidence for plume-involvement in the Palaeotethyan extensional regime during the Middle and Late Triassic. International Journal of Earth Sciences 98, 367–385.
Seltmann, R., Porter, T.M., 2005. The porphyry Cu–Au/Mo deposits of Central Eurasia 1. Tectonic, geologic and metallogenic setting, and significant deposits. In: Porter, T.M. (Ed.), Super Porphyry Copper & Gold Deposits: A Global Perspective, vol. 2. PGC Publishing, Adelaide, Australia, pp. 467–512.
Sengör, A.M.C., Natal'in, B.A., Burtman, U.S., 1993. Evolution of the Altaid tectonic collage and Paleozoic crustal growth in Eurasia. Nature 364, 209–304.
Shatagin, K.N., Degtyarev, K.E., Golubevt, V.N., Astrakhantsev, O.V., Kuznetsov, N.B., 2001. Vertical and lateral heterogeneity of the crust beneath Northern Kazakhstan from geochronological and isotopic–geochemical data on Paleozoic granitoids. Geotectonics 35, 356–372.
Shatov, V., Seltmann, R., Kremenetsky, A., Lehmann, B., Popov, V., Ermolov, P. (Eds.), 1996. Granite-related Ore Deposits of Central Kazakhstan and Adjacent Areas. Glagol Publ. House, St. Petersburg, p. 396.
Shen, P., Shen, Y.C., Liu, T.B., Li, G.M., Zeng, Q.D., 2007. Genesis of volcanic-hosted gold deposits in the Sawur gold belt, northern Xinjiang, China: evidence from REE, stable isotopes, and noble gas isotopes. Ore Geology Review 32, 207–226.
Shen, P., Shen, Y.C., Liu, T.B., Li, G.M., Zeng, Q.D., 2008a. Geology and geochemistry of the Early Carboniferous Eastern Sawur caldera complex and associated gold epithermal mineralization, Sawur Mountains, Xinjiang, China. Journal of Asian Earth Sciences 32, 259–279.
Shen, P., Shen, Y.C., Liu, T.B., Lu, J.J., Wei, J.P., Song, G.X., Meng, L., 2008b. Late Paleozoic gold and copper mineralization and tectonic evolution in Northwestern Xinjiang, China. Acta Petrologica Sinica 24, 1087–1100 (in Chinese with English abstract).
Shen, P., Shen, Y.C., Liu, T.B., Meng, L., Dai, H.W., Yang, Y.H., 2009. Geochemical signature of porphyries in the Baogutu porphyry copper belt, western Junggar, NW China. Gondwana Research 16, 227–242.
Shen, P., Shen, Y.C., Liu, T.B., Pan, H.D., Meng, L., Song, G.X., Dai, H.W., 2010a. Discovery of the Xiemisitai copper deposit in Western Junggar, Xinjiang and its geological significance. Xinjiang Geology 28, 413–418 (in Chinese with English abstract).
Shen, P., Shen, Y.C., Pan, H.D., Wang, J.B., Zhang, R., Zhang, Y.X., 2010b. Baogutu porphyry Cu–Mo–Au deposit, West Junggar, Northwest China: petrology, alteration, and mineralization. Economic Geology 105, 947–970.
Shen, P., Shen, Y.C., Wang, J.B., Zhu, H.P., Wang, L.J., Meng, L., 2010c. Methane-rich fluid evolution of the Baogutu porphyry Cu–Mo–Au deposit, Xinjiang, NW China. Chemical Geology 275, 78–98.
Shen, Y.C., Jin, C.W., 1993. Magmatism and Gold Mineralization in Western Junggar. Beijing Science Press, pp. 113–172 (in Chinese with English abstract) p.
Stacey, J.S., Kramers, J.D., 1975. Approximation of terrestrial lead isotope evolution by a two-stage model. Earth and Planetary Science Letters 26, 207–221.
Steiger, R.H., Jäger, E., 1977. Subcommission on geochronology: convention of the use of decay constants in geo- and cosmochronology. Earth and Planetary Science Letters 36, 359–362.
Sun, M., Yuan, C., Xiao, W.J., Long, X.P., Xia, X.P., Zhao, G.C., Lin, S.F., Wu, F.Y., Kröner, A., 2008. Zircon U–Pb and Hf isotopic study of gneissic rocks from the Chinese Altai: progressive accretionary history in the early to middle Paleozoic. Chemical Geology 247, 352–383.
Sun, S.S., McDonough, W.F., 1989. Chemical and isotopic sys-tematics of oceanic basalts: implications for mantle composition and processes. In: Saunders, A.D., Norry, M.J. (Eds.), Magmatism in Ocean Basins. Special Publication. Geological Society of London, pp. 313–345.
Vladimirov, A.G., Kruk, N.N., Khromykh, S.V., Polyansky, O.P., Chervov, V.V., Vladimirov, V.G., Travin, A.V., Babin, G.A., Kuibida, M.L., Khomyakov, V.D., 2008. Permian magmatism and lithospheric deformation in the Altai caused by crustal and mantle thermal process. Russian Geology and Geophysics 49, 468–479 (in Russian).
Wang, G.R., 1996. Classification of tectonic units and geologic evolution in the northern Xinjiang and neighboring area. Xinjiang Geology 14 (1), 12–27 (in Chinese with English abstract).
Wang, J.B., Wang, Y.W., Wang, L.J., 2004. The Junggar immature continental crust province and its mineralization. Acta Geologica Sinica (English edition) 78, 337–344.
Wiedenbeck, M., Alle, P., Corfu, F., Griffin, W.L., Meier, M., Oberli, F., Vonquadt, A., Roddick, J.C., Speigel, W., 1995. Three natural zircon standards for U–Th–Pb, Lu–Hf, trace-element and REE analyses. Geostandards Newsletter 19, 1–23.
Winchester, J.A., Floyd, P.A., 1977. Geochemical discrimination of different magma series and their differentiation products using immobile elements. Chemical Geology 20, 325–343.
Windley, B.F., Alexeiev, D., Xiao, W.J., Kröner, A., Badarch, G., 2007. Tectonic models for accretion of the Central Asian Orogenic Belt. Journal of the Geological Society of London 164, 31–47.
Wood, D.A., 1980. The application of a Th–Hf–Ta diagram to problems of tectonomagmatic classification and to establishing the nature of crustal contamination of basaltic lavas of the British Tertiary volcanic province. Earth and Planetary Science Letters 50, 11–30.
Wood, D.A., Joron, J.L., Treuil, M., 1979. A re-appraisal of the use of trace elements to classify and discriminate between magma series erupted in different tectonic settings. Earth and Planetary Science Letters 45, 326–336.
Xiao, W.J., Han, C.M., Yuan, C., Sun, M., Shoufa, L., Chen, H.L., Li, Z.L., Li, J.L., Sun, S., 2008. Middle Cambrian to Permian subduction-related accretionary orogenesis of Northern Xinjiang, NW China: implications for the tectonic evolution of central Asia. Journal of Asian Earth Sciences 32, 102–117.
Xiao, W.J., Huang, B.C., Han, C.M., Sun, S., Li, J.L., 2010. A review of the western part of the Altaids: a key to understanding the architecture of accretionary orogens. Gondwana Research. doi:10.1016/j.gr.2010.01.007.
Xiao, W.J., Kröner, A., Windley, B.F., 2009. Geodynamic evolution of Central Asia in the Paleozoic and Mesozoic. International Journal of Earth Sciences 98, 1185–1188.
Xinjiang Geological Bureau, 1979. 1:200000 Regional Geology Survey Reports. Geological Publishing House, Beijing (in Chinese).
Yakubchuk, A.S., Degtyarev, K.E., 1998. The character of link between the Chingiz and Boshchekul trends in the Caledonides of northeastern central Kazakhstan. Doklady Akademii Nauk 298, 1193–1198 (in Russian).
Zhang, J.E., Xiao, W.J., Han, C.M., Mao, Q.G., Ao, S.J., Guo, Q.Q., Ma, C., 2011. A Devonian to Carboniferous intra-oceanic subduction system in Western Junggar, NW China. Lithos. doi:10.1016/j.lithos.2011.03.013.
Zhang, R., Zhang, Y.X., Dong, G.S., Wang, J., Li, L.Q., 2006. Major breakthrough in copper exploration in the Baogutu porphyry copper deposit, western Junggar, Xinjiang, and its significance. Geology in China 33, 1354–1360 (in Chinese with English abstract).
Zhang, Y.Y., Guo, Z.J., 2010. New constraints on formation ages of ophiolites in northern Junggar and comparative study on their connection. Acta Petrologica Sinica 26, 421–430 (in Chinese with English abstract).
Zhou, T.F., Yuan, F., Fan, Y., Zhang, D.Y., Cooke, D., Zhao, G.C., 2008. Granites in the Saur region of the west Junggar, Xinjiang Province, China: geochronological and geochemical characteristics and their geodynamic significance. Lithos 106, 191–206.
Zhu, Y.F., Xu, X., 2006. The discovery of Early Ordovian ophiolite mélange in Taerbahatai Mts., Xinjiang, NW China. Acta Petrologica Sinica 22, 2833–2842 (in Chinese with English abstract).